Journal of Computer-Aided Molecular Design, **14:** 507–529, 2000.
KLUWER/ESCOM

Factor Xa: Simulation studies with an eye to inhibitor design

Xavier Daura[a], Eric Haaksma[b] & Wilfred F. van Gunsteren[a,*]
[a]*Laboratory of Physical Chemistry, Swiss Federal Institute of Technology Zürich, ETH Zentrum, CH-8092 Zürich, Switzerland;* [b]*Department of Chemical Research, Boehringer Ingelheim Pharma KG, D-88397 Biberach an der Riss, Germany*

Received 27 April 1999; Accepted 3 March 2000

Key words: biomolecular simulation, drug design, factor Xa, GROMOS, molecular dynamics

Summary

Factor Xa is a serine protease which activates thrombin and plays a key regulatory role in the blood-coagulation cascade. Factor Xa is at the crossroads of the extrinsic and intrinsic pathways of coagulation and, hence, has become an important target for the design of anti-thrombotics (inhibitors). It is not known to be involved in other processes than hemostasis and its binding site is different to that of other serine proteases, thus facilitating selective inhibition. The design of high-affinity selective inhibitors of factor Xa requires knowledge of the structural and dynamical characteristics of its active site. The three-dimensional structure of factor Xa was resolved by X-ray crystallography and refined at 2.2 Å resolution by Padmanabhan and collaborators. In this article we present results from molecular dynamics simulations of the catalytic domain of factor Xa in aqueous solution. The simulations were performed to characterise the mobility and flexibility of the residues delimiting the unoccupied binding site of the enzyme, and to determine hydrogen bonding propensities (with protein and with solvent atoms) of those residues in the active site that could interact with a substrate or a potential inhibitor. The simulation data is aimed at facilitating the design of high-affinity selective inhibitors of factor Xa.

Introduction

With vascular injury a series of processes are started, globally known as hemostasis, which serve to reduce and eventually stop loss of blood. One of these processes (secondary hemostasis) involves activation of the extrinsic and/or intrinsic pathways of coagulation. This leads to the production of insoluble fibrin, which is deposited into and about the platelet plug that occupies the site of vascular injury stabilising it and anchoring it. The extrinsic and intrinsic pathways of coagulation involve a series of coagulation factors acting in a sequence of reactions referred to as blood-coagulation cascade. The coagulation factors, which except for calcium and thromboplastin are proteins, circulate in the plasma as profactors and are activated within the corresponding pathway. The extrinsic pathway is initiated at a site of vascular injury in response to the release of tissue factor (factor III), while the intrinsic pathway is initiated by contact between blood and exposed endothelial cell surfaces in abnormal vessel walls. Factor Xa is the site at which the two pathways converge. Factor X is secreted into the blood as a zymogen (inactive proteolytic enzyme) and is converted to its active form, factor Xa, by the factor-VIIa/tissue-factor complex (in the extrinsic pathway) or by the factor-IXa/factor-VIIIa complex (in the intrinsic pathway). Factor Xa interacts with factor Va, calcium, and a phospholipid membrane surface to form the prothrombinase complex. This complex converts factor II (prothrombin) to factor IIa (thrombin), which then converts factor I (fibrinogen) to fibrin. In comparison to factor Xa alone, formation of the prothrombinase complex enhances the rate of prothrombin activation by about 10^5-fold [1].

An imbalance between clotting processes, clotting inactivation processes, and thrombolitic processes can lead to thrombotic or bleeding disorders. An-

*To whom correspondence should be addressed. E-mail: wfvgn@igc.phys.chem.ethz.ch

tithrombotics include inhibitors of thrombin, factor Xa [2], and factor IXa. Current antithrombotic therapies (mostly targetting thrombin) have limitations such as the need for clinical monitoring, failure to inhibit thrombin generation at the site of thrombus formation, lack of effectiveness towards inactivating clot-bound thrombin, and appearance of abnormal bleeding [3]. Further studies have suggested that inhibitors of factor Xa may have a reduced effect on abnormal bleeding when compared to direct or indirect inhibitors of thrombin [4, 5]. In addition, there is evidence that thrombin has other important functions in cellular [6, 7] and neurological processes [8–10]. Inhibition of factor Xa could thus offer a safety advantage over inhibition of thrombin.

The relatively recent release of three crystal structures of human factor Xa, des(1–45) factor Xa [11], des(1–45) factor Xa in complex with the synthetic inhibitor DX-9065a [12], and des(1–44) factor Xa in complex with the synthetic inhibitor FX-2212a [13], provides the possibility to apply structure-based drug design techniques to the development of specific inhibitors for this enzyme. Factor Xa consists of a light (A) chain (139 residues) and a heavy (B) chain (241 residues) linked by a single disulfide bond [11]. The light chain contains an N-terminal Gla domain and two epidermal growth factor (EGF)-like domains. The Gla domain (residues 1 to 45), absent in the crystals, contains 11 γ-carboxyglutamic acid residues and mediates binding to the negatively charged phospholipid membrane in the presence of Ca^{2+} ions. The EGF-like domains are involved in protein-protein interactions [14]. The heavy chain contains a trypsin-like serine protease domain, with an overall fold resembling that of chymotrypsin [11, 15, 16]. As with other serine proteases, like the B-chain of thrombin [17, 18], the residue numbering of the B-chain of factor Xa has been based on topological equivalences with chymotrypsin.

Similarly to trypsin, factor Xa cleaves its peptide substrates after basic arginine residues. Unlike trypsin, however, it has a high degree of specificity and cleaves only a limited number of peptide bonds at this residue. The active site of factor Xa is characterised by the catalytic triad His-57, Asp-102, and Ser-195, the specificity site (S1), with Asp-189, and the apolar or aryl-binding site (S4), with Tyr-99, Phe-174 and Trp-215. In the crystallographic structure of the apo form [11] the C-terminal region of the factor Xa A chain interacts in a substrate-like manner with the active site of a neighboring factor Xa molecule: Arg-439 from a factor Xa molecule occupies the S1 specificity site of another molecule making a hydrogen bonded ion pair with Asp-189. This arginine binding interaction is eliminated in the factor-Xa/DX-9065a and factor-Xa/FX-2212a structures [12, 13]. The aryl-binding site is not solely hydrophobic in character: The carbonyl oxygen atoms of Lys-96 and Glu-97 together with the Glu-97 side chain, at the edge of the S4 site, form a 'cation hole' [12] which can interact with positively charged groups. Although the chemical structure and the binding mode of the two inhibitors DX-9065a and FX-2212a are different, neither inhibitor interacts directly with the S2 and S3 sites [12, 13], in contrast to the majority of inhibitor complexes with serine proteases. As the S2 site is blocked by the side chain of Tyr-99, consistently with the selectivity of factor Xa for glycine in position P2, it seems to be not readily available for inhibitor binding. The S3 site, in which the P3 residue of the substrate makes an antiparallel β-ladder with Gly-216, was not involved in inhibitory binding either. Additional interactions with an inhibitor may involve Gln-192 [12, 13, 19–21] and Glu217 [22], at the entrance of the specificity site.

Except for the absence of the Tyr-60A–Thr-60I insertion loop (present in thrombin), the active site region of factor Xa resembles that of thrombin closely [11, 23]. The only sequence differences occur in the Leu99Tyr and Ile174Phe aliphatic to aromatic substitutions in the apolar site (S4) region of factor Xa. As these two residues are also different in other serine proteases, such as trypsin [24], the aryl-binding site provides an ideal target for the design of high-affinity selective factor Xa inhibitors.

The literature on factor Xa is extense – a search for articles with a title containing 'factor Xa' in the Citation Database of the Institute for Scientific Information [25] results in about 760 hits, with main contributions from experimental studies but also from combined experimental and theoretical studies [22, 26, 27] and theoretical studies alone [28–30]. Despite the almost untractable amount of information, there are, to our knowledge, no molecular dynamics simulation studies of the uncomplexed catalytic domain of factor Xa focusing at the dynamics and solvation of the unoccupied active site. In a rather general approach to exploring possible modes of interaction between factor Xa and a putative inhibitor, all the essential information could presumably be abstracted from the crystallographic structure of factor Xa and its comparison to the existing crystallographic structures of factor-Xa/inhibitor complexes [2, 21]. Further details

on specificity could be attained by comparison to complexes of other trypsin-like serine proteases with their own specific inhibitors and with factor-Xa-specific inhibitors [31, 32]. Existing data from mutation and enzymatic studies could give additional indication of the involvement of particular residues in binding and specificity [19, 20, 33]. Even though the crystallographic data carries little information about dynamics, and differences in structure and dynamics may exist between the crystal and solution states, some information on flexibility can be obtained via the above mentioned comparisons. However, while this is a sound approach it will only shed light on binding modes that are exploited by the actual inhibitors for which the structure of the complex is known. Information on the flexibility of particular residues in the active site of factor Xa will only show up as far as the docking of the inhibitor exploits this flexibility in complexes with known structure. Furthermore, information on solvation of the active site, e.g. average number of water molecules, their average residence times, and location of stable water sites, often critical in both substrate and inhibitory binding, is present only in a limited way in the crystallographic data and therefore not necessarily fully representative of the solution situation. All this missing information can, in principle, be obtained from molecular dynamics (MD) simulations. MD simulations of the uncomplexed catalytic domain of factor Xa will provide inhibitor-independent, and hence general-use, information on the mobility and flexibility of the active-site residues as well as on active-site solvation and location of stable water sites.

In this article we present results from two molecular dynamics simulations of the catalytic domain (B-chain) of factor Xa in aqueous solution. The first one is a 1-ns standard MD simulation, whereas in the second one a conformational-search enhancement technique called local-elevation search [34] is used to extend the conformational sampling of two side chains, Tyr-99 and Phe-174, of the S4 binding site within the 0.5-ns simulation period. The specific objectives of this study are: (i) To characterise the mobility and flexibility of the residues inside and at the borders of the unoccupied aryl-binding site (S4), (ii) to determine hydrogen-bonding propensities of key residues in the active site, i.e. residues which due to their relative position in the active site may interact with a potential inhibitor, and (iii) to identify stable water sites which could be replaced by, or bridge, inhibitor-protein interactions. A more general but equally important objective of this study is to illustrate the potential of this type of approach – investigation of mobility and flexibility of active-site residues and mapping of potential interaction sites with a putative inhibitor via MD simulation of the uncomplexed enzyme, which is not new but certainly underexploited in the field of drug design. For the system discussed here, and with the crystallographic coordinates of the apo-factor Xa as the only external input, this approach has provided information which is concurrent with that attained from the analysis of the crystallographic structures of factor-Xa/inhibitor complexes and mutation data.

Computational methods

Substitution of loop residues His-145 to Gln-151

The coordinates used as starting point for this study were extracted from the Brookhaven Protein Data Bank, entry 1*hcg* [11]. There are no coordinates for residues Glu-146 to Gln-151 in this entry. These residues are in the external loop Arg-143–Lys-156, corresponding to the position of the autolysis loop of thrombin and of the B/C chain cleavage of chymotrypsin. The final electron density map did not have density corresponding to Glu-146–Gln-151, and had relatively poor density for the side chains of Thr-144–His-145 and Ser-152–Arg-154 (an artificial B-factor of 0.5 nm^2 was assigned to all the atoms of His-145). This was a consequence of proteolytic cleavages in this region in the crystal used to collect the X-ray diffraction data [11]. Unfortunately, the crystallographic structures of the active-site-inhibited factor Xa were not available when the present study was started and structural modelling of the loop was, therefore, required. However, modelling of the structure of a loop of a protein is not without problems. If the modelled conformation of the loop would be very distinct from the native conformation its (unphysical) effect on local dynamics could be bigger than the effect of shortening the loop by the six undefined residues (His-145 to Gln-151, with a gap corresponding to position 148 [11]). For this reason, and because the loop does not directly interact with residues in the active site, we decided to substitute residues His-145 to Gln-151 with the shortest possible poly-glycine bridge. Thus, a three-glycine residue chain was modelled to bridge residues Thr-144 and Ser-152. The polypeptide chain studied hence consisted of 238 residues (Table 1).

Table 1. Amino acid sequence of factor Xa, after substitution of residues His-145–Gln-151 by three glycine residues

SN[a]	PDB[b]	RN[c]	SN[a]	PDB[b]	RN[c]	SN[a]	PDB[b]	RN[c]	SN[a]	PDB[b]	RN[c]	SN[a]	PDB[b]	RN[c]
1	16	Ile	51	65	Lys	101	115	Arg	151	166	Asn	201	214	Ser
2	17	Val	52	66	Val	102	116	Met	152	167	Ser	202	215	Trp
3	18	Gly	53	67	Arg	103	117	Asn	153	168	Cys	203	216	Gly
4	19	Gly	54	68	Val	104	118	Val	154	169	Lys	204	217	Glu
5	20	Gln	55	69	Gly	105	119	Ala	155	170	Leu	205	218	Gly
6	21	Glu	56	70	Asp	106	120	Pro	156	171	Ser	206	220	Cys
7	22	Cys	57	71	Arg	107	121	Ala	157	172	Ser	207	221	Ala
8	23	Lys	58	72	Asn	108	122	Cys	158	173	Ser	208	222	Arg
9	24	Asp	59	73	Thr	109	123	Leu	159	174	Phe	209	223	Lys
10	25	Gly	60	74	Glu	110	124	Pro	160	175	Ile	210	223A	Gly
11	26	Glu	61	75	Gln	111	124A	Glu	161	176	Ile	211	224	Lys
12	27	Cys	62	76	Glu	112	125	Arg	162	177	Thr	212	225	Tyr
13	28	Pro	63	77	Glu	113	126	Asp	163	178	Gln	213	226	Gly
14	29	Trp	64	78	Gly	114	127	Trp	164	179	Asn	214	227	Ile
15	30	Gln	65	79	Gly	115	128	Ala	165	180	Met	215	228	Tyr
16	31	Ala	66	80	Glu	116	129	Glu	166	181	Phe	216	229	Thr
17	32	Leu	67	81	Ala	117	130	Ser	167	182	Cys	217	230	Lys
18	33	Leu	68	82	Val	118	131	Thr	168	183	Ala	218	231	Val
19	34	Ile	69	83	His	119	131A	Leu	169	184	Gly	219	232	Thr
20	35	Asn	70	84	Glu	120	131B	Met	170	185	Tyr	220	233	Ala
21	36	Glu	71	85	Val	121	132	Thr	171	185A	Asp	221	234	Phe
22	37	Glu	72	86	Glu	122	133	Gln	172	185B	Thr	222	235	Leu
23	38	Asn	73	87	Val	123	134	Lys	173	186	Lys	223	236	Lys
24	39	Glu	74	88	Val	124	135	Thr	174	187	Gln	224	237	Trp
25	40	Gly	75	89	Ile	125	136	Gly	175	188	Glu	225	238	Ile
26	41	Phe	76	90	Lys	126	137	Ile	176	189	Asp	226	239	Asp
27	42	Cys	77	91	His	127	138	Val	177	190	Ala	227	240	Arg
28	43	Gly	78	92	Asn	128	139	Ser	178	191	Cys	228	241	Ser
29	44	Gly	79	93	Arg	129	140	Gly	179	192	Gln	229	242	Met
30	45	Thr	80	94	Phe	130	141	Phe	180	193	Gly	230	243	Lys
31	46	Ile	81	95	Thr	131	142	Gly	181	194	Asp	231	244	Thr
32	47	Leu	82	96	Lys	132	143	Arg	182	195	Ser	232	245	Arg
33	48	Ser	83	97	Glu	133	144	Thr	183	196	Gly	233	246	Gly
34	49	Glu	84	98	Thr	134		Gly	184	197	Gly	234	247	Leu
35	50	Phe	85	99	Tyr	135		Gly	185	198	Pro	235	248	Pro
36	51	Tyr	86	100	Asp	136		Gly	186	199	His	236	249	Lys
37	52	Ile	87	101	Phe	137	152	Ser	187	200	Val	237	250	Ala
38	53	Leu	88	102	Asp	138	153	Thr	188	201	Thr	238	251	Lys
39	54	Thr	89	103	Ile	139	154	Arg	189	202	Arg			
40	55	Ala	90	104	Ala	140	155	Leu	190	203	Phe			
41	56	Ala	91	105	Val	141	156	Lys	191	204	Lys			
42	57	His	92	106	Leu	142	157	Met	192	205	Asp			
43	58	Cys	93	107	Arg	143	158	Leu	193	206	Thr			
44	59	Leu	94	108	Leu	144	159	Glu	194	207	Tyr			
45	60	Tyr	95	109	Lys	145	160	Val	195	208	Phe			
46	61	Gln	96	110	Thr	146	161	Pro	196	209	Val			
47	61A	Ala	97	111	Pro	147	162	Tyr	197	210	Thr			
48	62	Lys	98	112	Ile	148	163	Val	198	211	Gly			
49	63	Arg	99	113	Thr	149	164	Asp	199	212	Ile			
50	64	Phe	100	114	Phe	150	165	Arg	200	213	Val			

[a]Sequence number used in the simulations.
[b]Sequence number in the Protein Data Bank (PDB) entry 1*hcg* [11].
[c]Three-letter code residue name.

Molecular system

The molecular model was taken from the GROMOS96 43A1 force field [35]. In this force field the aliphatic hydrogen atoms are treated as united atoms together with the carbon atom to which they are attached [35, 36]. The coordinates of polar hydrogen atoms (bound to nitrogen or oxygen) and aromatic hydrogen atoms of factor Xa were generated from standard geometries. For His-83, His-91, and His-199 the tautomer Nϵ_2-H was chosen, for it is slightly preferred energetically [37] and it would favour hydrogen-bond interactions in its conformation in the crystal. For His-57, involved in catalysis, the Nδ_1-H tautomer was chosen. The charge state of the ionizable groups was chosen to be that corresponding to a pH of 7.

Factor Xa was placed at the centre of a periodic truncated-octahedral box of length 7.70 nm between square planes and 6.67 nm between hexagonal planes. The minimum distance from any protein atom to the box wall in this initial configuration was 1.20 nm (the longest protein axis was 5.30 nm). The solvent was introduced into the box by using as a building block a cubic configuration of 216 equilibrated SPC [38] water molecules. All water molecules with the oxygen atom lying within 0.23 nm of a non-hydrogen protein atom were then removed. In this way a total of 6456 water molecules were introduced into the system. Truncated-octahedral periodic boundary conditions were applied. A steepest-descent energy minimisation of the system was performed in order to relax the first shells of water molecules around the protein. The protein atoms were positionally restrained using a harmonic interaction with a force constant of 25 kJ mol^{-1} nm^{-2}. Following this, a steepest-descent energy minimisation of the system without restraints was performed to eliminate any residual strain. The energy minimisations were terminated when the energy change per step became smaller than 0.1 kJ mol^{-1}.

Simulation setup

A 1 ns MD simulation at 298 K and 1 atm was then started. The initial velocities of the atoms were taken from a Maxwell-Boltzmann distribution at 100 K. The temperature of the system was kept at 100 K during the first 5 ps, and then raised to 298 K by successive 50 K increments over 5 ps intervals. The temperature and the pressure were maintained to the desired values by means of temperature and pressure baths [39]. The temperature of the protein and the solvent were independently, weakly coupled to the temperature bath with a relaxation time of 0.1 ps. The pressure of the system (calculated through a molecular virial) was weakly coupled to the pressure bath with isotropic scaling and a relaxation time of 0.5 ps. An estimated value of 45.75×10^{-5} (kJ mol^{-1} nm^{-3})$^{-1}$ was taken for the isothermal compressibility of the system at 298 K and 1 atm [35]. Bond lengths were constrained to ideal values [35] using the SHAKE algorithm [40] with a geometric tolerance of 10^{-4}. The time step for the leap-frog integration scheme was set to 2 fs. The non-bonded interactions were evaluated by means of a twin-range method: The short-range van der Waals and electrostatic interactions were evaluated at every time step by using a charge-group pair list that was generated with a short-range cut-off radius of 0.8 nm. Longer-range van der Waals and electrostatic interactions (between charge groups at a distance longer than the short-range cut-off and shorter than a long-range cut-off of 1.4 nm) were evaluated every 5 time steps, at which point the pair list was also updated, and were kept unchanged between these updates. The cut-off radii were applied to the centres of geometry of the solute charge groups and to the oxygen atoms of the water molecules.

A second MD simulation, 0.5 ns long, was carried out using a conformational-search enhancement technique called local elevation [34]. In this simulation a local-elevation interaction was applied to the χ_1 and χ_2 torsional angles of the side chains of Tyr-99 and Phe-174 in the aryl-binding site (S4) of factor Xa. Its aim was to investigate the changes in the protein's active-site structure that would be induced by a variation of these torsional angles. Using the local-elevation interaction, higher energy regions of conformational space become accessible to the side-chain torsional angles by energetically penalizing conformations that have been sampled before. This penalization is carried out gradually during the simulation by locally elevating the energy surface around each conformation that is visited. A given conformation is here defined by the combination of angles (or angle segments) of the four torsional angles selected. A Gaussian form was chosen for the local elevation interaction [34, 35]. The range of possible values (360°) of each dihedral was split in 16 segments of 22.5°. A force constant of 50 kJ mol^{-1} was chosen for the local elevation interaction, which implies an energy penalty of 20 k_BT per resampling of a conformation (angle segments). The two simulations were performed with the GROMOS96 package of programs [35, 41].

Analysis

The analysis was performed on the ensemble of system configurations extracted at 0.5-ps time intervals from the simulation. The first 200 ps of the simulation (equilibration) were excluded from the calculation of average properties. Least-squares fitting of atomic coordinates for the calculation of global properties, i.e. atom-positional root-mean-square deviation or difference (RMSD) and atomic B-factors of all protein atoms, was based on the backbone atoms of the secondary structure elements of factor Xa, calculated for the crystallographic structure with the program PROCHECK [42]. Least-squares fitting of atomic coordinates for the calculation of atom-positional RMSD values and atomic B-factors of selected atoms in the active site was based on a set of 48 backbone atoms from the active site region, residues in Table 4 plus Phe-174.

B-factors

Atomic isotropic B-factors were calculated from the simulations as described in Reference 35.

Hydrogen bonds

The geometry of a hydrogen bond is defined by a minimum donor–hydrogen–acceptor angle of 135° and a maximum hydrogen–acceptor distance of 0.25 nm. For the hydrogen-bond lifetime analysis a time resolution of 2 ps was chosen, which is less than the rotational correlation time of SPC water (3.4 ps [43]). Hydrogen bonds which were broken and reformed between the same partners within 2 ps were counted as single continuous hydrogen bonds, while those present for a shorter period were not included in the lifetime analysis. The same resolution was applied to the water-bridge lifetime analysis. Average hydrogen-bonding water sites and their corresponding B-factors were calculated by averaging the position of all water molecules hydrogen bonded to each donor and acceptor protein atom (of those selected) at all time frames, after superimposing the corresponding protein moieties for minimum atom-positional RMS differences.

Results and discussion

Global properties

General features of the dynamics of factor Xa in the 1-ns simulation are shown in Figures 1 and 2. The intramolecular (protein) interaction energy plus the interaction energy between the protein and the solvent is shown as a function of simulation time in Figure 1a. The sum of these energies fluctuates around an approximate value of -40500 kJ mol^{-1}. The atom-positional RMSD from the initial structure (PDB entry 1*hcg* [11]) of the backbone atoms and of all atoms of the protein are displayed in Figure 1b as a function of simulation time. The RMSD values rise in the initial 200 ps to 0.18 nm for the backbone and 0.26 nm for all atoms, and become approximately stable at around 0.2 nm for the backbone and 0.3 nm for all atoms after the initial 500 ps. The secondary structure of the protein is indicated in Figure 2 (left-hand panel) as a function of residue number (see Table 1) and simulation time. The secondary structure elements present in the crystallographic structure are in general stable along the 1-ns simulation. The crystallographically refined B-factors and the B-factors derived from the atom-positional fluctuations in the simulation in solution are also shown in Figure 2 (right-hand panel) for the Cα atoms. We note that a direct comparison between B-factors obtained from X-ray diffraction data and from simulation is of limited value, considering the very different environments, time scales, system sizes, and determination techniques [44]. Therefore, the values shown here should only be considered as indicative of the differences in mobility between different segments of the protein chain. For obvious reasons, there are no experimental B-factors for the three glycine residues bridging Thr-144 and Ser-152 (see Table 1). Except for Gln-133, which has a simulated B-factor markedly higher than the three crystallographic B-factors, the relative B-factors between different segments of the protein chain show a reasonable correspondence between simulation and experiment.

Dynamical properties of selected active-site residues

The flexibility of the three aromatic residues in the aryl-binding site, Tyr-99, Phe-174, and Trp-215, determines to which extent this site can accommodate different inhibitor shapes. Additionally, residue Glu-97 at the edge of the aryl-binding site and residues

Table 2. Comparison of simulation-derived and crystallographically refined B-factors of residues Tyr-99, Phe-174, Trp-215, Glu-97, Gln-192, and Glu-217, in and around the aryl-binding site

Residue	Atom	B-factor (nm^2)			
		Simulation	Crystal A[a]	Crystal B[b]	Crystal C[c]
99Tyr	Cα	0.07	0.17	0.21	0.12
	Cβ	0.11	0.16	0.19	0.09
	Cγ	0.09	0.17	0.16	0.08
	$C\delta_1$	0.16	0.17	0.15	0.08
	$C\delta_2$	0.29	0.16	0.16	0.06
	$C\epsilon_1$	0.19	0.17	0.15	0.08
	$C\epsilon_2$	0.38	0.15	0.17	0.07
	Cζ	0.21	0.19	0.18	0.08
	Oη	0.35	0.21	0.18	0.11
174Phe	Cα	0.16	0.17	0.35	0.13
	Cβ	0.30	0.17	0.35	0.12
	Cγ	0.45	0.16	0.35	0.11
	$C\delta_1$	0.65	0.16	0.36	0.12
	$C\delta_2$	0.59	0.21	0.36	0.12
	$C\epsilon_1$	0.95	0.17	0.37	0.11
	$C\epsilon_2$	0.85	0.20	0.38	0.12
	Cζ	1.00	0.16	0.36	0.12
215Trp	Cα	0.05	0.16	0.28	0.05
	Cβ	0.07	0.15	0.26	0.04
	Cγ	0.07	0.14	0.23	0.02
	$C\delta_1$	0.10	0.10	0.22	0.02
	$C\delta_2$	0.08	0.17	0.23	0.02
	$N\epsilon_1$	0.12	0.13	0.21	0.02
	$C\epsilon_2$	0.11	0.15	0.22	0.02
	$C\epsilon_3$	0.12	0.17	0.24	0.02
	$C\zeta_2$	0.16	0.14	0.20	0.02
	$C\zeta_3$	0.19	0.14	0.23	0.02
	$C\eta_2$	0.20	0.17	0.22	0.03
97Glu	Cα	0.18	0.22	0.43	0.24
	Cβ	0.28	0.22	0.48	0.27
	Cγ	0.42	0.22	0.54	0.31
	Cδ	0.92	0.26	0.57	0.35
	$O\epsilon_1$	1.68	0.27	0.58	0.35
	$O\epsilon_2$	1.67	0.30	0.58	0.34
192Gln	Cα	0.08	0.30	0.27	0.11
	Cβ	0.12	0.30	0.29	0.14
	Cγ	0.47	0.35	0.32	0.19
	Cδ	0.53	0.37	0.34	0.23
	$O\epsilon_1$	0.73	0.40	0.36	0.25
	$N\epsilon_2$	0.76	0.38	0.34	0.27
217Glu	Cα	0.17	0.19	0.33	0.09
	Cβ	0.25	0.20	0.35	0.09
	Cγ	0.34	0.22	0.39	0.10
	Cδ	0.18	0.23	0.40	0.11
	$O\epsilon_1$	0.29	0.22	0.40	0.14
	$O\epsilon_2$	0.16	0.19	0.38	0.11

[a]Data from the Protein Data Bank (PDB)-entry 1*hcg*, apo-factor Xa [11].
[b]Data from the PDB-entry 1*fax*, the factor-Xa/DX-9065a complex [12].
[c]Data from the PDB-entry 1*xka*, the factor-Xa/FX-2212a complex [13].

Table 3. Intramolecular hydrogen bonds of 36 selected protein atoms

Donor/acceptor[a]	Donor/acceptor	Simulation (%)[b]	Crystal A[c,d]	Crystal B[c,e]	Crystal C[c,f]
57His-NH	102Asp-Oδ_1	99	+	+	+
57His-Nδ_1Hδ_1	102Asp-Oδ_1	70	−	+	+
	102Asp-Oδ_2	66	+	+	+
57His-Nϵ_2	–	–	−	−	−
96Lys-O	99Tyr-NH	23	−	−	−
97Glu-Oϵ_1	97Glu-NH	17	−	−	−
97Glu-Oϵ_2	97Glu-NH	11	−	−	−
97Glu-O	–	–	−	−	−
98Thr-O	–	–	−	−	−
99Tyr-NH	96Lys-O	23	−	−	−
	95Thr-O	–	−	+	−
99Tyr-Oη	–	–	−	−	−
99Tyr-OηHη	–	–	−	−	−
99Tyr-O	215Trp-Nϵ_1Hϵ_1	68	−	−	−
102Asp-NH	–	–	−	−	−
102Asp-Oδ_1	56Ala-NH	10	−	−	−
	57His-NH	99	+	+	+
	57His-Nδ_1Hδ_1	70	−	+	+
102Asp-Oδ_2	56Ala-NH	74	−	−	−
	57His-Nδ_1Hδ_1	66	+	+	+
	214Ser-OγHγ	99	−	−	−
102Asp-O	229Thr-Oγ_1Hγ_1	83	+	+	+
175Ile-O	–	–	−	−	−
189Asp-Oδ_1	190Ala-NH	40	−	−	+
189Asp-Oδ_2	190Ala-NH	15	−	−	−
	221Ala-NH	92	+	−	+
192Gln-Oϵ_1	–	–	−	−	−
192Gln-Nϵ_2Hϵ_{21}	–	–	−	−	−
192Gln-Nϵ_2Hϵ_{22}	–	–	−	−	−
195Ser-Oγ	193Gly-NH	36	−	−	−
195Ser-OγHγ	–	–	−	−	−
214Ser-Oγ	215Trp-NH	17	−	−	−
	229Thr-Oγ_1Hγ_1	11	−	−	−
214Ser-OγHγ	102Asp-Oδ_2	99	−	−	−
214Ser-O	–	–	−	−	−
215Trp-NH	214Ser-Oγ	17	−	−	−
	227Ile-O	–	+	−	+
215Trp-Nϵ_1Hϵ_1	99Tyr-O	68	−	−	−
215Trp-O	227Ile-NH	96	+	+	+
216Gly-NH	–	–	−	−	−
216Gly-O	–	–	−	−	−
217Glu-Oϵ_1	173Ser-NH	40	−	−	−
	173Ser-OγHγ	91	−	−	−
	224Lys-NζHζ	–	−	+	−
217Glu-Oϵ_2	172Ser-OγHγ	92	−	−	−
	173Ser-NH	83	+	+	+
218Gly-NH	–	–	−	−	−
218Gly-O	–	–	−	−	−

[a] Selected atoms from the region of the active site.
[b] Percentage of time a particular hydrogen bond is found in the simulation. Only hydrogen bonds that are present at least 10% of the time are shown.
[c] Presence (+) or absence (−) of a hydrogen bond.
[d] Data derived from the coordinates in the Protein Data Bank (PDB)-entry 1*hcg*, apo-factor Xa [11].
[e] Data derived from the coordinates in the PDB-entry 1*fax*, the factor-Xa/DX-9065a complex [12].
[f] Data derived from the coordinates in the PDB-entry 1*xka*, the factor-Xa/FX-2212a complex [13].

Table 4. Hydrogen bonds of 36 selected protein atoms with water

Donor/acceptor[a]	Occ[b] (%)	Mul[c] (%)	⟨lt⟩[d] (ps)	Max(lt)[e] (ps)	B-factor[f] (nm^2)	Crystal A[g] (O number)[i]	Crystal C[h] (O number)[i]
57His-NH	–					–	–
57His-Nδ_1Hδ_1	–					–	–
57His-Nϵ_2	94	23	13	211	0.34	–	518/519/520
96Lys-O	57	1	6	20	0.99	631	582
97Glu-Oϵ_1	87	214	4	40	5.50	560	–
97Glu-Oϵ_2	89	224	6	32	5.26	560	–
97Glu-O	77	33	4	22	2.02	634	–
98Thr-O	53	3	6	31	3.14	518/600	578
99Tyr-NH	32	0	8	32	0.39	–	–
99Tyr-Oη	55	15	6	33	1.59	719/816	–
99Tyr-OηHη	97	0	27	125	1.76	–	519
99Tyr-O	71	1	10	100	0.49	537	683/684
102Asp-NH	79	0	14	108	0.10	516	684
102Asp-Oδ_1	14	0	28	99	0.10	–	–
102Asp-Oδ_2	–					–	–
102Asp-O	–					–	–
175Ile-O	59	5	14	159	1.23	518	578
189Asp–Oδ_1	92	193	7	47	2.38	514	516
189Asp–Oδ_2	95	119	12	430	1.25	672	513/514
192Gln-Oϵ_1	72	24	5	22	4.67	–	–
192Gln-Nϵ_2Hϵ_{21}	79	0	6	28	2.03	564	587
192Gln-Nϵ_2Hϵ_{22}	84	0	9	69	2.78		
195Ser-Oγ	13	0	5	20	1.30	–	–
195Ser-OγHγ	89	0	42	180	0.17	–	518/520
214Ser-Oγ	–					–	–
214Ser-OγHγ	–					537	683
214Ser-O	80	6	6	46	0.86	–	518
215Trp-NH	–					–	–
215Trp-Nϵ_1Hϵ_1	–					–	–
215Trp-O	11	0	2	6	0.16	522	–
216Gly-NH	72	1	6	25	0.59	737	–
216Gly-O	76	22	4	24	1.39	604/653/737	–
217Glu-Oϵ_1	95	104	12	67	2.02	–	–
217Glu-Oϵ_2	91	32	11	59	1.13	543	–
218Gly-NH	94	0	41	272	1.62	653	–
218Gly-O	45	12	3	22	3.76	540/604	513

[a] Selected atoms from the region of the active site.
[b] Percentage of time a particular atom is hydrogen bonded with water in the simulation (only shown if larger than 10%).
[c] Percentage of multiple hydrogen bonds with water; e.g. 0% if the given atom never has more than one hydrogen bond with water at the same time and 100% if it has an average of 2 hydrogen bonds with water at the same time (counting only those configurations in which it has at least one hydrogen bond with water).
[d] Average lifetime of hydrogen bonds with water (see Methods).
[e] Maximum observed lifetime of hydrogen bonds with water.
[f] B-factor of the hydrogen-bonding water site (see Methods).
[g] Data derived from the coordinates in the Protein Data Bank (PDB)-entry 1*hcg*, apo-factor Xa [11].
[h] Data derived from the coordinates in the PDB-entry 1*xka*, the factor-Xa/FX-2212a complex [13].
[i] Water-oxygen sequence number in the PDB entry. To identify possible hydrogen bonds between donor water-oxygen atoms and acceptor protein atoms in a crystallographic structure, a maximum distance donor-acceptor criterium of 0.35 nm was used. To identify hydrogen bonds between donor protein atoms and acceptor water-oxygen atoms, coordinates for the polar hydrogen atoms of the protein were first generated according to standard geometries [35], and maximum distance and minimum angle criteria were then applied as described in the Methods section.

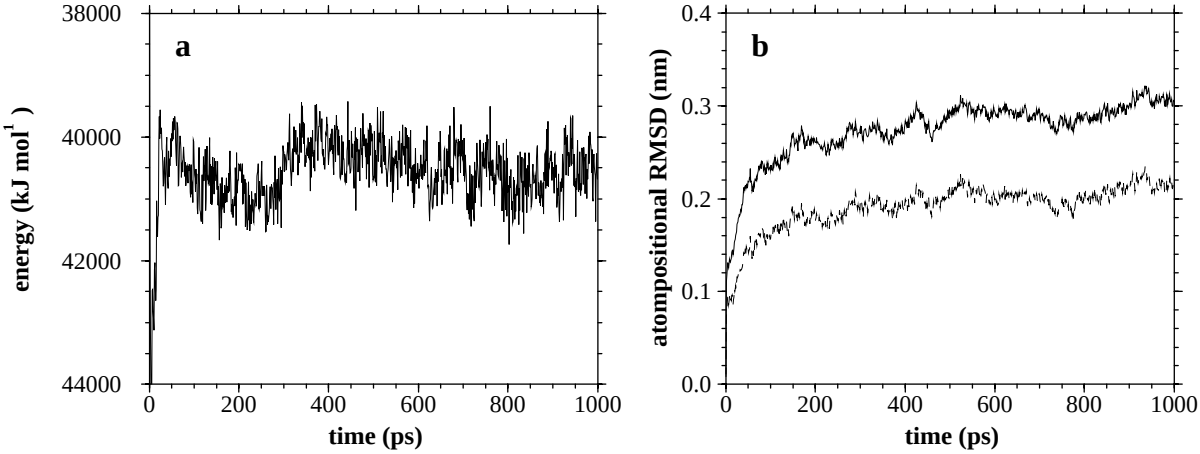

Figure 1. (a) Energy of protein intramolecular interactions plus protein–water interactions as a function of simulation time. (b) Atom-positional RMSD from the initial (apo-factor Xa) crystallographic structure [11] as a function of simulation time. Dashed line: RMSD of backbone atoms; solid line: RMSD of all atoms.

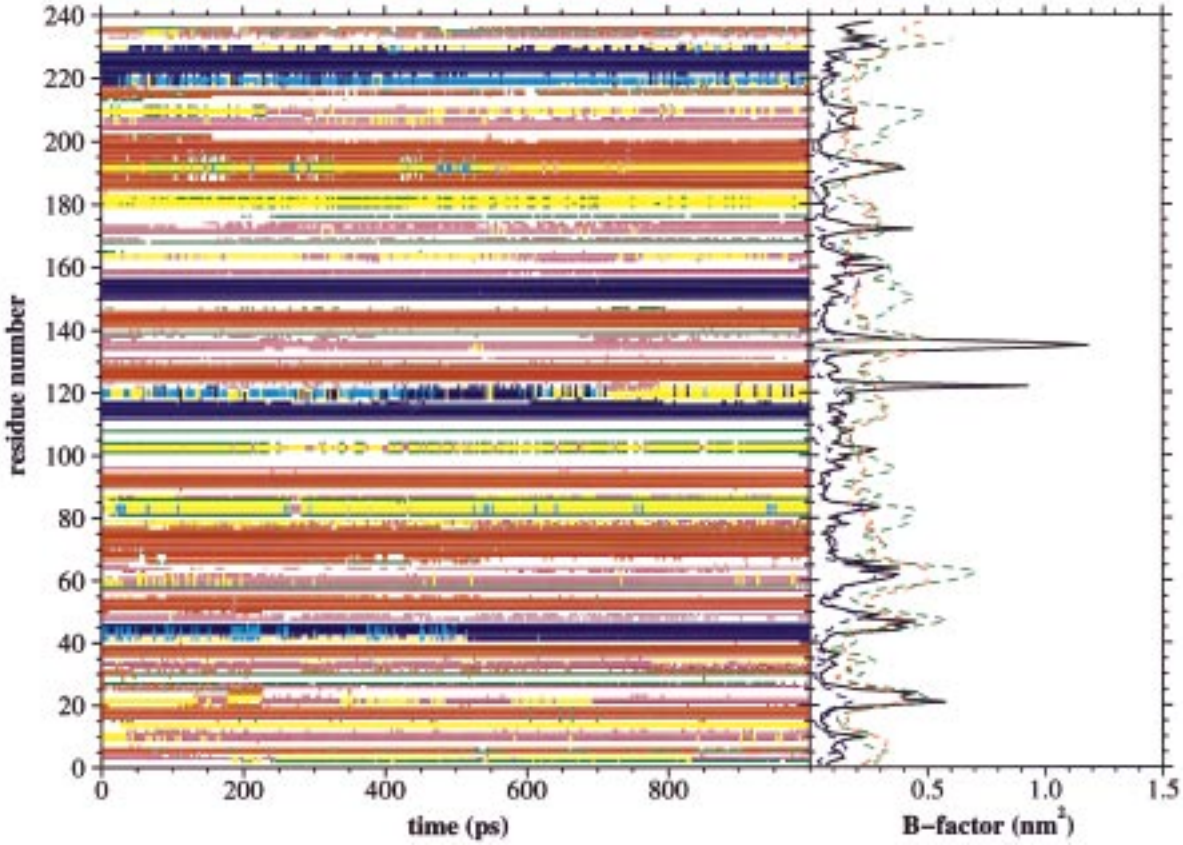

Figure 2. Left-hand panel: Secondary structure as a function of time. Red: extended strand participating in β-ladder; brown: bend; yellow: hydrogen-bonded turn; green: β-bridge; dark blue: α-helix; light blue: 3_{10}-helix; according to definitions of secondary structure by Kabsch and Sander [45], calculated with the program PROCHECK [42]. Right-hand panel: B-factors of the Cα atoms as derived from simulation (black, solid line) and X-ray diffraction data (dashed lines). B-factors from the apo-factor Xa crystal [11] in red, from the factor-Xa/DX-9065a crystal [12] in green, and from the factor-Xa/FX-2212a crystal [13] in blue. Residue numbers in these plots do not correspond to residue numbers in 1*hcg* (PDB entry), but to a sequential numbering from 1 to 238 (see Table 1 for conversion).

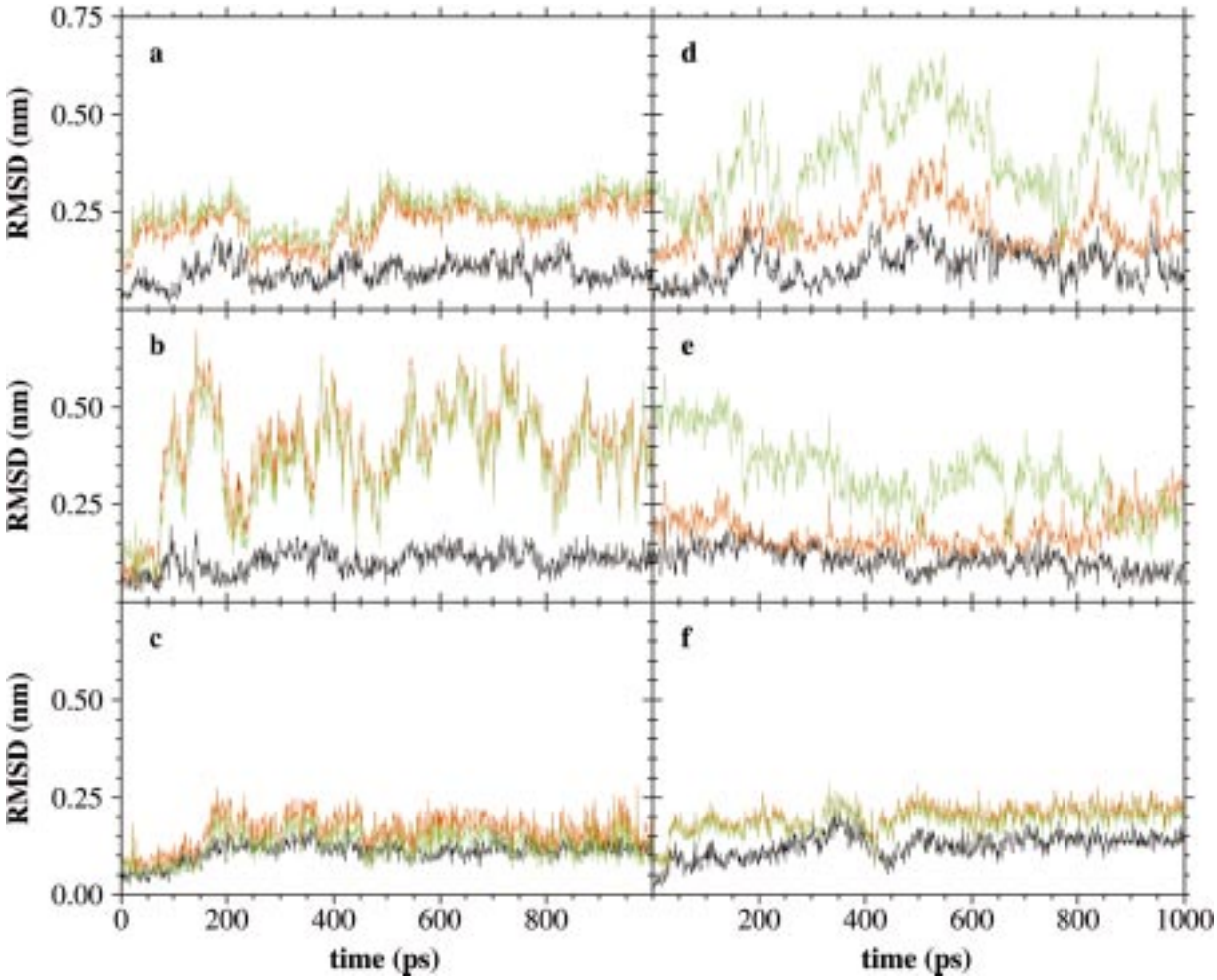

Figure 3. Atom-positional root-mean-square deviation (RMSD) from the apo-factor Xa [11] and factor-Xa/DX-9065a [12] crystallographic structures as a function of simulation time, of residues Tyr-99 (a), Phe-174 (b), Trp-215 (c), Glu-97 (d), Gln-192 (e), and Glu-217 (f). Black: RMSD of the backbone atoms from the positions in the apo-factor Xa structure; red: RMSD of the side chain atoms from the positions in the apo-factor Xa structure; green: RMSD of the side chain atoms from the positions in the factor-Xa/DX-9065a structure.

Gln-192 and Glu-217 at the entrance of the specificity site have been found to change conformation upon inhibitor binding, contributing to the network of intermolecular interactions. In the crystallographic structure of the complex between factor Xa and the inhibitor DX-9065a [12], Gln-192 moves with respect to its position in the apo-factor Xa structure [11] toward the naphthamidine group of the inhibitor. The pyrrolidine ring of DX-9065a is almost completely buried by a perpendicular 'two-sandwich' [12] arrangement: The aromatic rings of Phe-174 and Tyr-99 are both parallel to the pyrrolidine ring, while the aliphatic part of the Glu-97 side chain and the indole ring of Trp-215 cover the pyrrolidine group from perpendicular planes. In this arrangement the side chains of Phe-174, Tyr-99 and, especially, Glu-97 deviate from the conformations adopted in the apo-factor Xa structure. However, the side chain of Glu-97 was not perfectly defined in the complex and can probably adopt more than one conformation [12]. In the crystallographic structure of the complex between factor Xa and the inhibitor FX-2212a [13], Gln-192 moves toward the biphenyl ring of the inhibitor to a position similar to that observed in the factor-Xa/DX-9065a crystal. The pyridine ring of FX-2212a is located in the centre of the aryl-binding site and parallel to the indole ring of Trp-215. The side chains of Tyr-99 and Phe-174 conserve the conformations observed in the apo-factor Xa crystal, while the side chain of Glu-97 moves toward the inhibitor to approximately the same position

adopted in the factor-Xa/DX-9065a structure. In none of the previous factor-Xa/inhibitor complexes does the side chain of Glu-217 move away from its position in the apo-factor Xa structure, nor does it directly interact with the inhibitors. However, Shaw et al. [22] have suggested, on the basis of modelling studies, that the higher potency of the (*Z*,*Z*) isomer of the factor-Xa inhibitor BABCH with respect to its (*E*,*E*) and (*E*,*Z*) isomers could be due to the formation of an extra salt bridge between one of the benzamidines of the (*Z*,*Z*) isomer and the side chain of Glu-217, which would change conformation upon binding.

Three types of analysis have been performed to characterise the mobility and flexibility of the side chains of Tyr-99, Phe-174, Trp-215, and Glu-97 in the aryl-binding site and Gln-192 and Glu-217 at the entrance of the specificity site in the MD simulation in solution: (i) calculation of RMSD from the crystallographic atomic positions, (ii) atomic isotropic B-factors, and (iii) χ_1 and χ_2 side-chain dihedral angles. The RMSD from the initial (apo-factor Xa crystallographic) positions of the backbone atoms and side-chain atoms of the above-mentioned residues are displayed in Figure 3 as a function of simulation time. The average RMSD (from 200 ps to 1000 ps) of the backbone atoms and side-chain atoms are, respectively, 0.10 nm and 0.22 nm for Tyr-99, 0.11 nm and 0.41 nm for Phe-174, 0.12 nm and 0.17 nm for Trp-215, 0.12 nm and 0.22 nm for Glu-97, 0.10 nm and 0.17 nm for Gln-192, and 0.13 nm and 0.21 nm for Glu-217. The RMSD from the crystallographic atomic positions in the two factor-Xa/inhibitor complexes (PDB entries 1*fax* [12] and 1*xka* [13]) were also calculated. Backbone RMSDs from the three sets of crystallographic coordinates are visually undistinguishable for these six residues. Thus, only the backbone RMSD from the atomic positions in the apo-factor Xa structure is displayed in Figure 3. Side-chain RMSDs from the atomic positions in the two factor-Xa/inhibitor structures are also indistinguishable and, therefore, only the side-chain RMSD from the atomic positions in the factor-Xa/DX-9065a structure is displayed in Figure 3. As expected, given the small positional differences of the three aromatic residues in the three crystallographic structures, the time series of the side-chain RMSDs from the atomic positions in the two factor-Xa/inhibitor structures and in the apo-factor Xa structure are very similar for these three residues (Figure 3a–c). The side chain of Phe-174 deviates most from its crystallographic position. This is not surprising, as in the absence of a substrate or an inhibitor the phenylalanine is, of the three, the residue with more free space around to move, being almost completely exposed to the solvent. On the other hand, the side chain of Trp-215 deviates least from its crystallographic position. Note that the RMSD values of the side-chain atoms are partially a consequence of the deviation from the initial structure of the backbone itself. The side chain of Glu-97 shows large displacements from the three reference crystallographic positions (Figure 3d), and clearly stays closer to its position in the apo-factor Xa structure than in the two factor-Xa/inhibitor structures. The side chain of Gln-217 undergoes a slow transition between its initial position, corresponding to the apo-factor Xa structure, and its position in the two factor-Xa/inhibitor structures (Figure 3e), ending at an RMSD-equidistant position from the two reference states. The RMSD of the side chain of Glu-217 from its crystallographic position – very similar in the three reference structures – is markedly stable (Figure 3f), indicating an early positional drift rather than a high-amplitude fluctuation.

The simulation and crystallographic B-factors of the Cα and non-hydrogen side-chain atoms of residues Tyr-99, Phe-174, Trp-215, Glu-97, Gln-192, and Glu-217 are shown in Table 2. The B-factors derived from the X-ray diffraction data are, in a rather systematic way, higher for the factor-Xa/DX-9065a complex than for the apo-factor Xa, and lowest for the factor-Xa/FX-2212a complex (see also right-hand panel of Figure 2). A second observation which warns against detailed comparison of simulation-derived and crystallographically refined B-factors is that the simulation B-factors of the Cα atoms are substantially smaller than the average simulation B-factors of the corresponding side-chains – as one would expect in solution – and often smaller than the crystallographic Cα B-factors, while crystallographic B-factors tend to be more homogeneous, i.e. with the B-factors of Cα atoms closer to the average B-factors of the corresponding side chains. The side chain of Trp-215 is the least mobile of the six side chains in Table 2, except in the factor-Xa/DX-9065a crystal. In this crystal Tyr-99 has the lowest B-factors. On the other end, the side chain of Glu-97 is the most mobile, with the exception of the apo-factor Xa crystal in which Gln-192 has the highest B-factors. The side chain of Phe-174 is in all four cases (simulation and crystals) the most mobile of the three aromatic side chains, although in the apo-factor Xa crystal Tyr-99 and Phe-174 have very similar B-factors. The side chain of Glu-217 is less mobile than the side chains of Glu-97 and Gln-192,

with the exception of the factor-Xa/DX-9065a crystal in which the side chain of Gln-192 has the lowest B-factors of the three. Figure 4 shows the average positions of the six residues in the simulation (from 200 to 1000 ps) with a colour-coded representation of the atomic B-factors.

The χ_1 and χ_2 torsional dihedral angles of the side chains of Tyr-99, Phe-174, and Trp-215 (between the Cα and Cβ atoms and between the Cβ and Cγ atoms, respectively) are plotted as a function of time in Figure 5. In general, the torsional angles of the three side chains are similar in the three crystallographic structures, with a maximum deviation of about 35° corresponding to the χ_2 angle of Tyr-99. The χ_1 torsional angle of Tyr-99 (Figure 5a) fluctuates around its initial (apo-factor Xa crystallographic) value of $-74°$ during the entire simulation. The values of the χ_1 angle of Tyr-99 in the factor-Xa/DX-9065a structure ($-106°$) and in the factor-Xa/FX-2212a structure ($-92°$) are also in the range covered by the fluctuations in the simulation. The χ_2 torsional angle (Figure 5b), however, rapidly changes from its initial value of 16° to $-90°$, and stays around this value during most of the simulation time. In Phe-174 both the χ_1 and χ_2 torsional angles (Figure 5c,d) oscillate around their respective initial values ($-55°$ and $-69°$) with sizable fluctuations, including some transitions (the transitions between consecutive minima being of 120° for the χ_1 torsional angle and of 60° for the χ_2 torsional angle). In Trp-215 the χ_1 and χ_2 torsional angles (Figures 5e,f) oscillate also around their respective initial values (58° and 91°), but with small-amplitude fluctuations. In order to see whether the motions of the three side chains are to some extent coupled in the simulation, three vectors were defined in each of the aromatic rings of Tyr-99, Phe-174, and Trp-215. Two (approximately) perpendicular vectors were defined in the plane of the ring, while the third vector was normal to this plane. A time crosscorrelation analysis of all pairs of vectors (from different residues) thus defined showed little correlation in the motions of the three aromatic systems (results not shown). The χ_1 and χ_2 torsional dihedral angles of the side chains of Glu-97, Gln-192, and Glu-217 are plotted as a function of time in Figure 6. The χ_1 torsional angle of Glu-97 (Figure 6a) fluctuates around a value of $-73°$, 25° lower than its initial (apo-factor Xa crystallographic) value. At two short time intervals in the simulation it also samples the angles corresponding to the factor-Xa/DX-9065a structure ($-162°$) and to the factor-Xa/FX-2212a structure ($-172°$). The χ_2 torsional angle (Figure 6b) is mostly distributed between its value in the apo-factor Xa structure ($-76°$) and in the factor-Xa/DX-9065a ($-302°$) and factor-Xa/FX-2212a ($-296°$) structures. The χ_1 torsional angle of Gln-192 (Figure 6c) deviates quickly from its initial value of $-136°$, to return later to a range of values between the value of $-60°$ observed in the factor-Xa/DX-9065a structure and the value of $-89°$ observed in the factor-Xa/FX-2212a structure. The χ_2 torsional angle (Figure 6d) drifts also rapidly from its initial value of $-135°$ and evolves to values around the $-178°$ corresponding to the factor-Xa/DX-9065a structure. The χ_1 torsional angle of Glu-217 (Figure 6e) stays in the simulation around its initial value of $-76°$. The χ_2 torsional angle (Figure 6f) changes from its initial value of 162° to values around 290°, returning only briefly to the χ_2 values corresponding to the three crystallographic structures.

Observation of the trajectory structures yields the following picture (see also Figure 4). The side chain of Trp-215 fluctuates around its initial (apo-factor Xa crystallographic) position, maintaining its relative orientation at the base of the aryl-binding site. The side chain of Tyr-99 moves slightly toward the backbone at residue Lys-96 with a 90° to 120° rotation of the aromatic ring, and fluctuates around this position during most of the simulation. This positional deviation from the initial structure seems to be partially driven by the interaction between the hydroxyl group of Tyr-99 and Lys-92. The neighbouring aromatic rings – including Tyr-60 and Phe-94 – probably contribute to stabilise the new side-chain conformation. Interestingly, a similar orientation of the side chain of Tyr-99 is found in the catalytic domains of single-chain human tissue-type plasminogen activator (sc-tPA) [46] and vampire-bat plasminogen activator (DSPAα_1) [47], two other chymotrypsin-like serine proteases. In the crystallographic structures of these enzymes the phenol ring of Tyr-99 is 90° rotated – with respect to the conformation in the factor Xa crystals – and parallel to the plane of the indole ring of Trp-215. Conversely, in the two-chain human tissue-type plasminogen activator (tc-tPA) [48, 49] the orientation of the side chain of Tyr-99 is as in the crystallographic structures of factor Xa. The side chain of Phe-174 has a large freedom of movement: It is almost completely exposed to the solvent and there is no obvious interaction that would restrict its position to the crystallographic one. Nevertheless, it never invades the cavity of the aryl-binding site, which remains always accessible. The side chain of Glu-97 is almost permanently oriented

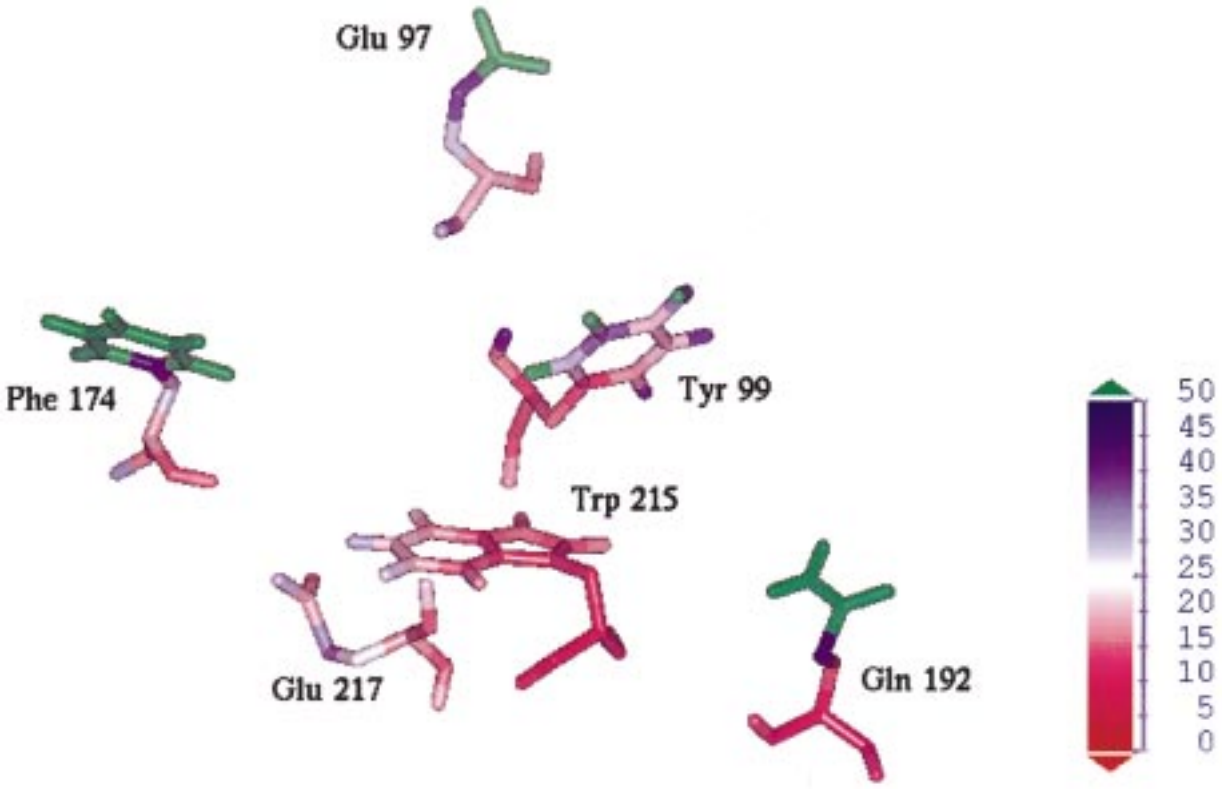

Figure 4. Schematic representation of the average atomic positions of residues Tyr-99, Phe-174, Trp-215, Glu-97, Gln-192, and Glu-217 in the simulation time interval from 200 ps to 1000 ps. The atoms are coloured according to their relative fluctuations, from red for B-factors of 0 $Å^2$ to green for B-factors of 50 $Å^2$ or higher.

to the solvent, much as in the apo-factor Xa structure, and never moves toward the cavity of the aryl-binding site as in the two factor-Xa/inhibitor structures. The side chain of Gln-192 drifts slowly toward the entrance of the S1 site, to a position similar to that adopted in the factor-Xa/inhibitor structures. The rotation of the χ_2 dihedral angle of Glu-217 leaves its carboxylate group slightly oriented toward the binding-site region, which makes the interaction between this group and a putative inhibitor, as described by Shaw et al. [22], plausible.

Hydrogen bonding and solvation of active-site residues

The degree of solvation of the aryl-binding site has been analysed by counting the number of water molecules present in its cavity as a function of simulation time (Figure 7a). Deformations of this cavity involving changes of volume are expected to reflect on the number of water molecules that can access it. The number of water molecules in the cavity of the aryl-binding site, in the period of time simulated, ranges from 1 to 13, but in general oscillates between 5 and 10 molecules. The average (7 molecules) remains close to the initial number of 9 water molecules. Note that the initial configuration of water molecules in the system did not originate from the crystal, but was generated with a space filling criterion [35]. The number of times (out of 1000 system configurations) a particular water molecule was found in the aryl-binding site is shown in Figure 7b as a function of the sequence numbers of the water molecules. The large number (195) of water molecules that access the aryl-binding site during 1 ns clearly indicates that the solvation of this cavity is highly dynamic, with (generally) short residence times for the individual water molecules. Of the 195 water molecules that visited the aryl-binding site, only 16 stayed in it for 10% to 20% of the simulation time, one stayed for 27% of the simulation time, and one stayed for 70% of the simulation time.

Knowledge of the hydrogen-bonding trends of potential donors and acceptors in the active site of factor

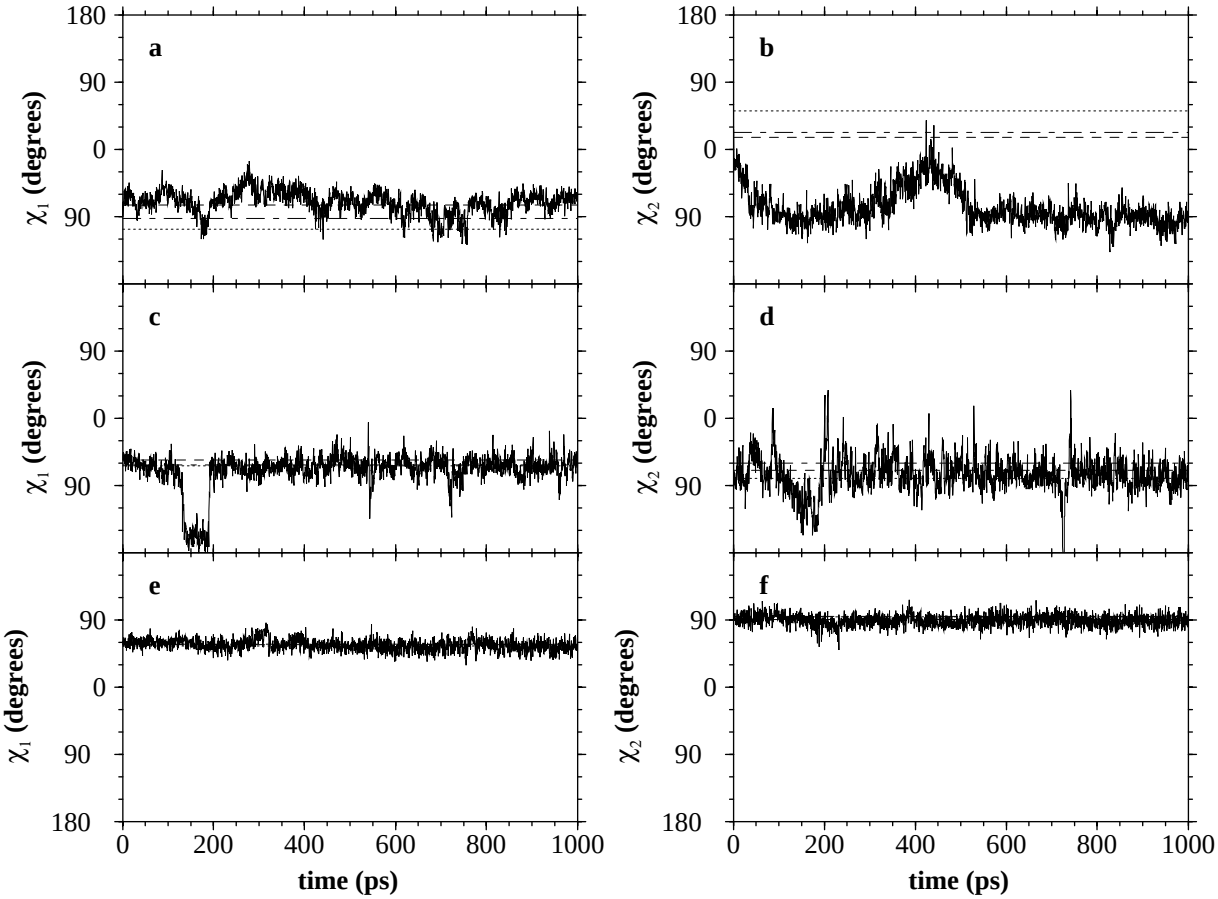

Figure 5. χ_1 and χ_2 torsional angles of the side chains of residues Tyr-99, Phe-174, and Trp-215 as a function of simulation time. (a) χ_1 of Tyr-99; (b) χ_2 of Tyr-99; (c) χ_1 of Phe-174; (d) χ_2 of Phe-174; (e) χ_1 of Trp-215; (f) χ_2 of Trp-215. Dashed line: torsional-angle value in the apo-factor Xa crystallographic structure; dotted line: torsional-angle value in the factor-Xa/DX-9065a crystallographic structure; dot-dashed line: torsional-angle value in the factor-Xa/FX-2212a crystallographic structure.

Xa is of key importance to the design of specific interactions between this enzyme and new model inhibitors. Thirty-six potential donors and acceptors of hydrogen bonds from the region of the active site of factor Xa were selected, and their hydrogen-bonding trends in the simulation were analysed. The intramolecular (protein–protein) hydrogen bonds formed by these 36 atoms and their occurrences (in percentage of time) are shown in Table 3, together with their occurrence in the three crystallographic structures. Hydrogen bonds with an occurrence higher than 50% in the simulation are: 57His-Nδ_1Hδ_1–102Asp-Oδ, 57His-NH–102Asp-Oδ_1, 56Ala-NH–102Asp-Oδ_2, 214Ser-OγHγ–102Asp-Oδ_2, and 229Thr-Oγ_1Hγ_1–102Asp-O in the catalytic site and its vicinity, 215Trp-Nϵ_1Hϵ_1–99Tyr-O in the aryl-binding site, 173Ser-NH–217GluOϵ, 173Ser-OγHγ–217Glu-Oϵ_1, and 172Ser-OγHγ–217Glu-Oϵ_2 at the side of the aryl-binding site, 227Ile-NH–215Trp-O at the entrance to the specificity site, and 221Ala-NH–189Asp-Oδ_2 in the specificity site. The hydrogen bonds that are present in at least two of the three crystallographic structures are also present with a high occurrence in the simulation, with the exception of the hydrogen bond 215Trp-NH–227Ile-O.

Hydrogen-bonding trends of the 36 selected atoms with water are shown in Table 4. For each atom, the occurrence (in percentage of time) of hydrogen bonds with water, the percentage of multiple hydrogen bonds with water, the average and maximum lifetime of hydrogen bonds with water, and the B-factor for the corresponding average water position, are given as calculated from the trajectory (water-molecule unspecific). Hydrogen bonds with crystallographic waters in

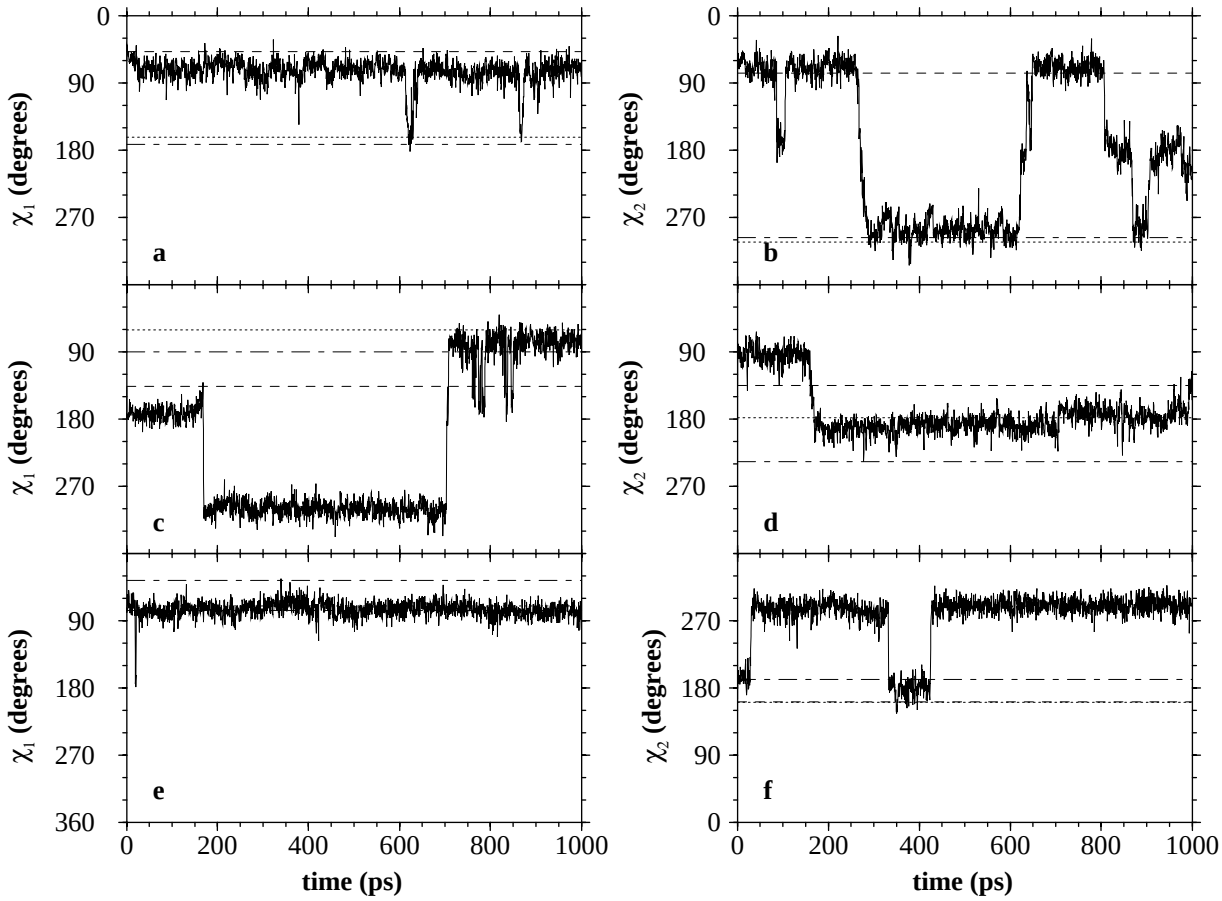

Figure 6. χ_1 and χ_2 torsional angles of the side chains of residues Glu-97, Gln-192, and Glu-217 as a function of simulation time. (a) χ_1 of Glu-97; (b) χ_2 of Glu-97; (c) χ_1 of Gln-192; (d) χ_2 of Gln-192; (e) χ_1 of Glu-217; (f) χ_2 of Glu-217. Dashed line: torsional-angle value in the apo-factor Xa crystallographic structure; dotted line: torsional-angle value in the factor-Xa/DX-9065a crystallographic structure; dot-dashed line: torsional-angle value in the factor-Xa/FX-2212a crystallographic structure.

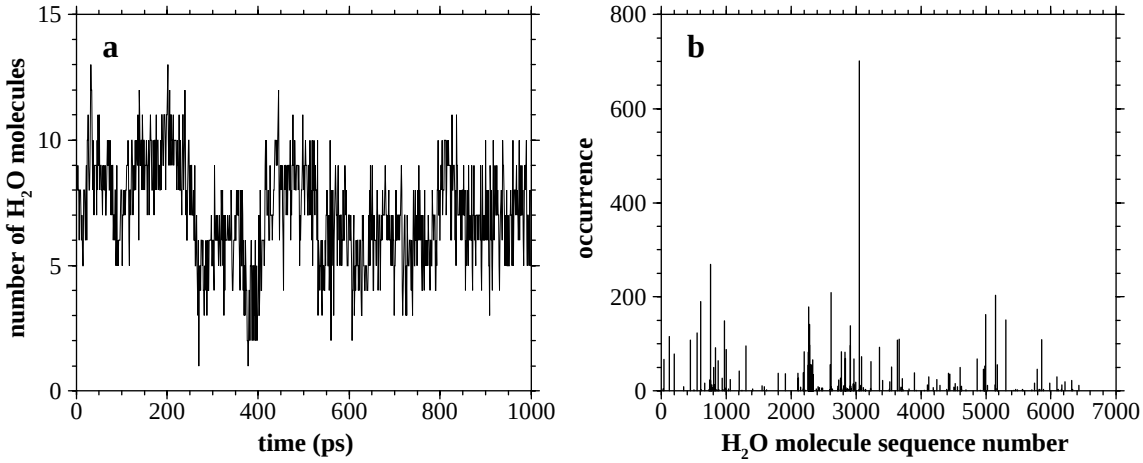

Figure 7. (a) Number of water molecules in the aryl-binding pocket as a function of simulation time. A water molecule was considered to be in the aryl-binding pocket if the distance between its oxygen and each of the Cβ atoms of Tyr-99, Phe-174 and Trp-215 was smaller than 0.9 nm. (b) Number of times each of the water molecules in the system has been found in the aryl-binding pocket in 1000 system configurations taken at 1 ps intervals.

Table 5. Water bridges between 36 selected protein atoms

Donor/acceptor[a]	Donor/acceptor[a]	Occ[b] (%)	⟨lt⟩[c] (ps)	Max(lt)[d] (ps)	Crystal A[e] (O number)[g]	Crystal C[f] (O number)[g]
57His-Nϵ_2	99Tyr-OηHη	–			–	519
57His-Nϵ_2	195Ser-OγHγ	73	17	140	–	518/520
57His-Nϵ_2	214Ser-O	–			–	518
97Glu-Oϵ_1	97Glu-Oϵ_2	41	2	7	560	–
98Thr-O	175Ile-O	–			518	578
99Tyr-O	102Asp-NH	56	8	50	–	684
99Tyr-O	214Ser-OγHγ	–			537	683
189Asp-Oδ_1	189Asp-Oδ_2	39	3	11	–	–
189Asp-Oδ_2	218Gly-NH	52	40	147	–	–
189Asp-Oδ_2	218Gly-O	–			–	513
195Ser-OγHγ	214Ser-O	–			–	518
216Gly-NH	216Gly-O	–			737	–
216Gly-O	217Glu-Oϵ_2	27	6	20	–	–
216Gly-O	218Gly-O	–			604	–
216Gly-O	218Gly-NH	–			653	–

[a]From the set of 36 atoms from the region of the active site (see Table 4).
[b]Percentage of time the two atoms are bridged by a water molecule in the simulation (only shown if larger than 10%).
[c]Average lifetime of the water bridge (see Methods).
[d]Maximum observed lifetime of the water bridge.
[e]Data derived from the coordinates in the Protein Data Bank (PDB)-entry 1*hcg*, apo-factor Xa [11] (see Table 4).
[f]Data derived from the coordinates in the PDB-entry 1*xka*, the factor-Xa/FX-2212a complex [13].
[g]Water-oxygen sequence number in the PDB entry.

the apo-factor Xa and factor-Xa/FX-2212a structures – PDB entries 1*hcg* and 1*xka*, respectively – are also indicated (water-molecule specific). The crystallographic structure of the factor-Xa/DX-9065a complex was refined without addition of water molecules [12]. Except for 99Tyr-O, 189Asp-Oδ, and 217Glu-Oϵ, the atoms that are highly involved in protein–protein hydrogen bonds are barely involved in protein–water hydrogen bonds. Atoms that are hydrogen bonded to water with a high occurrence (over 70%) are: 57His-Nϵ_2 and 195Ser-OγHγ in the catalytic site, 99Tyr-O, 102Asp-NH, and 214Ser-O in the vicinity of the catalytic site, 97Glu-O, 97Glu-Oϵ, and 99Tyr-OηHη in the aryl-binding site, 192Gln-Oϵ_1, 192Gln-Nϵ_2, 216Gly-NH, 216Gly-O, 217Glu-Oϵ, and 218Gly-NH at the entrance to the specificity site, and 189Asp-Oδ in the specificity site. The two 189Asp-Oδ atoms have on average two to three hydrogen bonds with water at a time. The two 97Glu-Oϵ atoms are also highly solvated – by around three water molecules at a time – but just as a consequence of being completely exposed to the solvent. The atoms that are hydrogen bonded to water with a minimum occurrence of 50% and longest average lifetimes (more than 20 ps) are: 99Tyr-OηHη, 195Ser-OγHγ and 218Gly-NH. It is important to note that the absolute lifetimes depend very much on the resolution at which the analysis is done. The atoms involved in hydrogen bonds (with a minimum occurrence of 50%) with very localised water positions (B-factor below 1.0 nm^2) are: 57His-Nϵ_2 and 195Ser-OγHγ in the catalytic site, 99Tyr-O, 102Asp-NH and 214Ser-O in the vicinity of the catalytic site, 96Lys-O in the aryl-binding site, and 216Gly-NH at the entrance of the specificity site. These atoms have also a water molecule within hydrogen-bonding distance in at least one of the two crystallographic structures. An approximate representation of the water sites described in Table 4 is given in Figure 8, with red spheres indicating conserved water sites in the simulation and blue spheres indicating the positions of crystallographic waters in the apo-factor Xa structure. Water bridges between pairs of atoms belonging to the set of 36 atoms from the region of the active site are shown in Table 5. Water bridges occur in the simulation between 57His-Nϵ_2 and 195Ser-OγHγ in the catalytic site, between 99Tyr-O and 102Asp-NH in the vicinity of the catalytic site, between 216Gly-O and 217Glu-Oϵ_2 at the entrance of the specificity

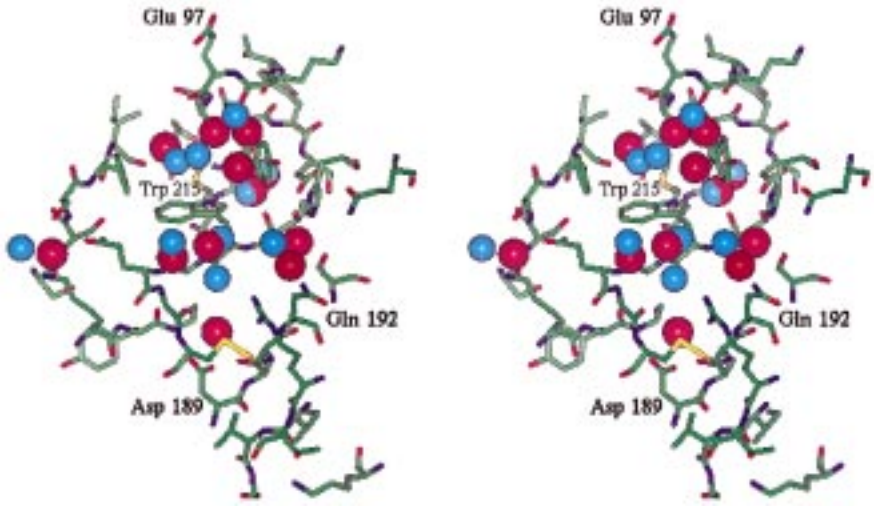

Figure 8. Schematic stereo representation of conserved water sites in the active site of the catalytic domain of factor Xa as observed in the simulation. The active site structure is taken from the apo-factor Xa crystallographic structure (Protein Data Bank-entry *1hcg* [11]). The blue spheres correspond to water positions in the same crystallographic structure. The red spheres correspond (approximately) to stable water sites in the simulation (see Table 4).

site, and between 189Asp-Oδ_2 and 218Gly-NH in the specificity site. Of these, only the water bridges between 57His-Nϵ_2 and 195Ser-OγHγ and 99Tyr-O and 102Asp-NH are also present in the crystallographic structure of factor-Xa/FX-2212a. Note that in the simulation the catalytic triad is connected through a direct hydrogen bond between 57His-Nδ_1Hδ_1 and 102Asp-Oδ ($\sim$70% occurrence, Table 3), which is also present in the two factor-Xa/inhibitor crystallographic structures, and a water bridge between 195Ser-OγHγ and 57HisNϵ_2 ($\sim$70% occurrence, Table 5), present also in the factor-Xa/FX-2212a crystallographic structure. It is worth stressing the presence of the water bridge between 217Glu-Oϵ_2 and 216Gly-O, which is only possible when the carboxylate group of Glu-217 is oriented toward the entrance of the specificity site, and thus available for specific interactions with a putative inhibitor. The water molecule that stays around 70% of the simulation time in the aryl-binding site (Figure 7b) is bound to the atoms 172Ser-Oγ, 174Phe-NH, 175Ile-NH, and 175Ile-O (not shown), that is, at one side of the aryl-binding pocket.

At this point it is worth commenting on the hydrogen-bonding interactions involved in the binding of the inhibitors DX-9065a and FX-2212a to the active site of factor Xa in the respective crystallographic structures. The discussion that follows is based on the analysis of both crystallographic structures with the exact criteria used in the simulation (see Methods) and, therefore, differences with the description of factor-Xa/inhibitor interactions in References 12 and 13 may exist. In the factor-Xa/DX-9065a crystal the binding in the S1 site involves formation of a salt bridge between the naphthamidine amidino group of the inhibitor and the carboxylate group of Asp-189. The orientation of the amidino group would allow a twin-twin arrangement if the side chain of Asp-189 was in the same conformation as in the apo-factor Xa structure [12]. However, the χ_2 torsional angle of Asp-189 rotates almost 90° with respect to its conformation in the apo-factor Xa crystallographic structure, resulting in a single 189Asp-Oδ_2–twin (amidino group) arrangement. Note a discrepancy between the naming of the Asp-189 carboxylate oxygens in the PDB entry 1*fax* – where Oδ_2 is the oxygen hydrogen-bonded to the naphthamidine amidino group of the inhibitor – and the naming in Reference 12 – where Oδ_1 is the oxygen hydrogen-bonded to the amidino group. The carbonyl oxygen of Gly-218 forms a hydrogen bond with the N_2 (naming in PDB entry 1*fax*) of the amidino group. Note that in Reference 12 this hydrogen bond is attributed to the carbonyl oxygen of Gly-219, but this residue is not in the sequence of factor Xa (see Table 1). In the aryl-binding site the NH of the acetimidoyl group of the inhibitor is within hydrogen-bonding distance from the Oϵ_2 carboxylate oxygen of Glu-97. In the factor-Xa/FX-2212a crystal the binding in the S1 site involves also formation of a salt bridge between the amidino group of FX-2212a and the carboxylate group of Asp-189, but in this case

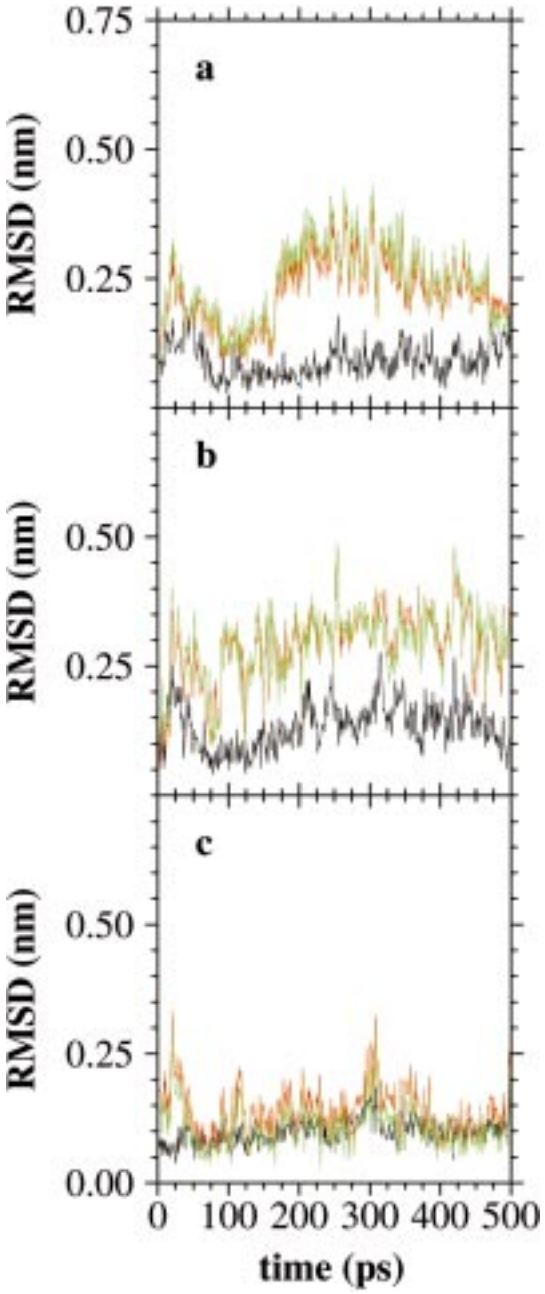

Figure 9. Atom-positional root-mean-square deviation (RMSD) from the apo-factor Xa [11] and factor-Xa/DX-9065a [12] crystallographic structures as a function of simulation time, of residues Tyr-99 (a), Phe-174 (b), and Trp-215 (c). Black: RMSD of the backbone atoms from the positions in the apo-factor Xa structure; red: RMSD of the side chain atoms from the positions in the apo-factor Xa structure; green: RMSD of the side chain atoms from the positions in the factor-Xa/DX-9065a structure. Simulation with local-elevation interaction (see Methods).

in a twin-twin geometry [13]. In the simulation the χ_2 torsional dihedral angle of Asp-189 fluctuates most of the time between the 4° of the factor-Xa/FX-2212a structure and the 53° of the factor-Xa/DX-9065a structure, and the χ_1 angle fluctuates closely around its (similar) values in the three crystallographic structures (data not shown). In the factor-Xa/FX-2212a structure the carbonyl oxygen of Gly-218 forms also a hydrogen bond with the N_2 (naming in PDB entry 1*xka*) of the amidino group of the inhibitor. The water molecule bridging 98Thr-O and 175Ile-O (Table 5) serves also as anchoring point for the inhibitor by interaction with the nitrogen atom of its pyridine ring. Overall, hydrogen bonds between the two inhibitors and the active site of factor Xa are thus heavily based on the carboxylate group of Asp-189 and the carbonyl group of Gly-218 in the specificity site.

Enhanced conformational search using local-elevation MD simulation

In order to investigate to which extent the side chains of Tyr-99 and Phe-174 could be forced to adopt conformations other than those observed in the crystal and in the equilibrium simulation in solution discussed above, *viz.* if inhibitors with markedly different shapes would be able to access the aryl-binding site, a 0.5-ns simulation was carried out with an external interaction (local-elevation interaction) acting on the χ_1 and χ_2 side-chain torsional dihedral angles of Tyr-99 and Phe-174 (see Methods). The RMSD from the initial (apo-factor Xa crystallographic) positions of the backbone atoms and side-chain atoms of residues Tyr-99, Phe-174, and Trp-215 are displayed in Figure 9 as a function of simulation time. The average RMSDs (from 200 ps to 500 ps) of the backbone atoms and side-chain atoms are, respectively, 0.09 nm and 0.26 nm for Tyr-99, 0.15 nm and 0.32 nm for Phe-174, and 0.11 nm and 0.14 nm for Trp-215. The side chain of Phe-174 (Figure 9b), although more mobile, deviates less from its initial conformation than in the 1-ns equilibrium simulation (Figure 3b). Besides that, no significant differences are observed between the two simulations in terms of RMSDs. The χ_1 and χ_2 torsional dihedral angles of the side chains of Tyr-99, Phe-174, and Trp-215 are plotted as a function of time in Figure 10. Clearly, rotation around the χ_1 and χ_2 torsional angles of Tyr-99 (Figures 10a, b) is still restricted despite the local-elevation driving force. Interestingly, the χ_2 dihedral of Tyr-99 rotates early in the simulation to angles around 120°, adopting an

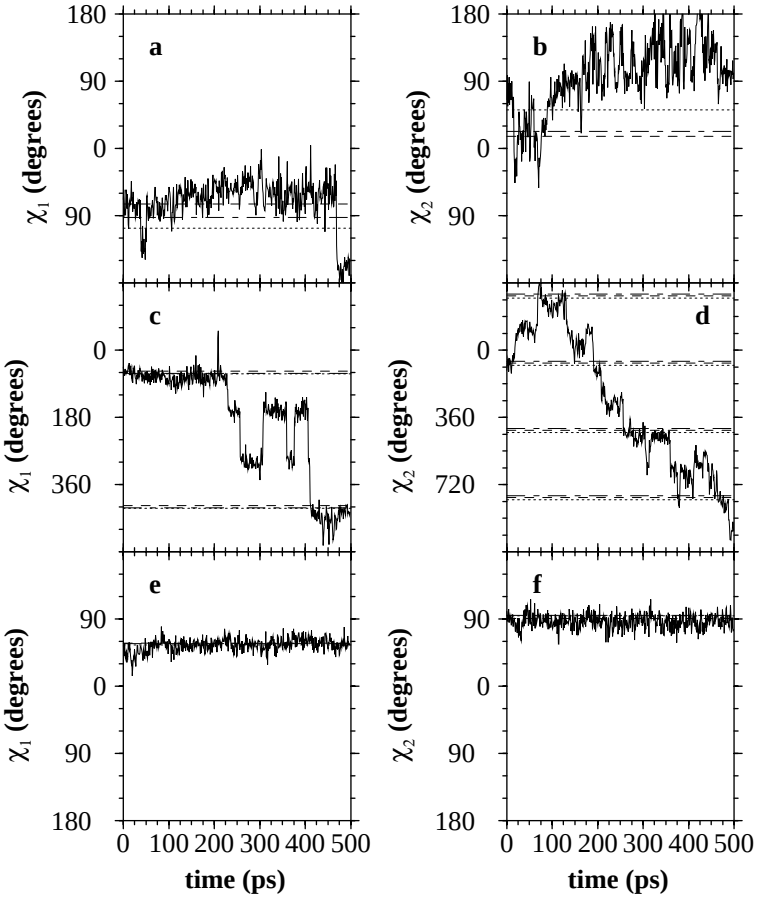

Figure 10. χ_1 and χ_2 torsional angles of the side chains of residues Tyr-99, Phe-174, and Trp-215 as a function of simulation time. (a) χ_1 of Tyr-99; (b) χ_2 of Tyr-99; (c) χ_1 of Phe-174; (d) χ_2 of Phe-174; (e) χ_1 of Trp-215; (f) χ_2 of Trp-215. Dashed line: torsional-angle value in the apo-factor Xa crystallographic structure; dotted line: torsional-angle value in the factor-Xa/DX-9065a crystallographic structure; dot-dashed line: torsional-angle value in the factor-Xa/FX-2212a crystallographic structure. Simulation with local-elevation interaction (see Methods).

orientation very similar to that predominant in the 1-ns equilibrium simulation, but with bigger fluctuations due to the local-elevation energy. Rotation around the χ_1 and χ_2 torsional angles of Phe-174 (Figures 10c, d) is substantially increased in this simulation. Indeed, most of the local-elevation energy is absorbed by the side-chain torsional angles of Phe-174, as a consequence of – or indicating – its large freedom of movement. The RMSDs from the initial positions of the backbone atoms and side-chain atoms of a subset of 16 active site residues (residues in Table 3 plus Phe-174) are plotted in Figure 11 as a function of time, together with the same quantity for the 1-ns equilibrium simulation. The RMSD curves corresponding to the simulation with local elevation show alternation of high- and low-RMSD time periods. This oscillatory behaviour is induced by the local elevation interaction applied to the χ_1 and χ_2 angles of Tyr-99 and Phe-174, which produces strain in their environment. Inspection of the structures of the trajectory shows that, unlike in the 1-ns equilibrium simulation, the side chain of Phe-174 often invades the cavity of the aryl-binding site. The increased motions of the side chains of Tyr-99 and, especially, Phe-174 do not perturb the position of the Trp-215 aromatic ring, but effectively reduce the water-accessible volume in the aryl-binding site. The number of water molecules accessing this cavity is shown as a function of time in Figure 12a. The average is around 5 water molecules, significantly below the observed average in the equilibrium simulation (7 water molecules). The number of times (out of 500 system configurations) a particular water molecule has been found in the aryl-binding site is shown in Figure 12b as a function of the sequence numbers of the

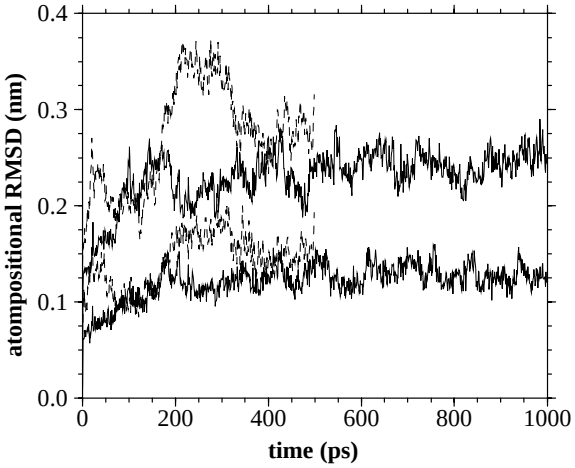

Figure 11. Root-mean-square deviation from the initial positions (apo-factor Xa crystallographic structure) of the backbone atoms and side chain atoms of a subset of 16 active-site residues (residues in Table 4 plus Phe-174) as a function of time. Solid lines: RMSD values from the 1-ns equilibrium simulation (the curve with lower values corresponding to the RMSD of backbone atoms); dashed lines: RMSD values from the 0.5-ns simulation with local elevation (the curve with lower values corresponding to the RMSD of backbone atoms).

water molecules. Of the 179 water molecules that visited the aryl-binding site – a number similar to the 195 that visited it in the equilibrium simulation but during half the simulation time – only 9 stayed in it for 10 to 20% of the simulation time.

Conclusions

A summary of the insights regarding the active site of the catalytic domain of factor Xa gained from the simulations discussed above is presented here. Special attention has been put to (i) the flexibility of the three aromatic residues delimiting the aryl-binding-site cavity, i.e. Tyr-99, Phe-174, and Trp-215, (ii) the conformational preferences of three residues located at the edges of the aryl-binding site and specificity site which could change conformation upon inhibitor binding [12, 13, 22], i.e. Glu-97, Gln-192, and Glu-217, and (iii) the solvation of the aryl-binding site and the presence of conserved water positions in the active site. The side chain of Phe-174 is the most flexible of the three aromatic residues in the aryl-binding site. In the 1-ns equilibrium simulation it searches conformational space with high motional freedom, and maintains no stable interactions with other protein residues. Nevertheless, it never invades the cavity of the aryl-binding site, which remains always accessible to water. In the 0.5-ns simulation with a local-elevation interaction acting on the χ_1 and χ_2 torsional dihedral angles of Tyr-99 and Phe-174, the side chain of the latter absorbes most of the energy pumped into these four degrees of freedom. This indicates that in this environment the rotational barriers are lower for the χ_1 and χ_2 torsional angles of Phe-174 than for the corresponding angles of Tyr-99. In both the equilibrium simulation and the simulation with local elevation Tyr-99 shows a clear preference for a conformation in which its side chain is oriented slightly toward the backbone at residue Lys-96, with a 90° to 120° rotation of the aromatic ring with respect to the crystallographic conformation [11–13]. A similar conformation of Tyr-99 has been observed in crystals of the catalytic domains of single-chain human tissue-type plasminogen activator (sc-tPA) [46] and vampire-bat plasminogen activator (DSPAα_1) [47]. This observation suggests that the sc-tPA and DSPAα_1 conformation of Tyr-99 could also be populated in the unoccupied aryl-binding site of the catalytic domain of factor Xa. The side chain of Trp-215 is stable in its crystallographic conformation, and is not perturbed by the higher mobility of the side chains of Tyr-99 and Phe-174 when the local-elevation interaction is applied. In the 1-ns equilibrium simulation the side chain of Glu-97 sticks out to the solvent as in the apo-factor Xa crystallographic structure, and never moves toward the cavity of the aryl-binding site as in the two factor-Xa/inhibitor structures. In the same simulation the side chain of Gln-192 drifts slowly toward the entrance of the specificity site, to a position similar to that adopted in the factor-Xa/inhibitor structures. The χ_2 torsional angle of Glu-217 rotates about 120° with respect to its value in the crystallographic structures and leaves the carboxylate group slightly oriented toward the entrance to the specificity site, which makes the interaction between this group and a putative inhibitor, as described by Shaw et al. [22], plausible. This is further supported by the presence of a water bridge between the Oϵ_2 carboxylate oxygen of Glu-217 and the carbonyl oxygen of Gly-216, at the entrance of the specificity site. The cavity of the aryl-binding site is permanently solvated in the 1-ns equilibrium simulation by an average number of seven water molecules. Although the solvation of the cavity is highly dynamic, i.e. there is a fast exchange with the solvent at the surface of the protein and water molecules are rarely trapped in the cavity, there are a number of conserved water sites. These

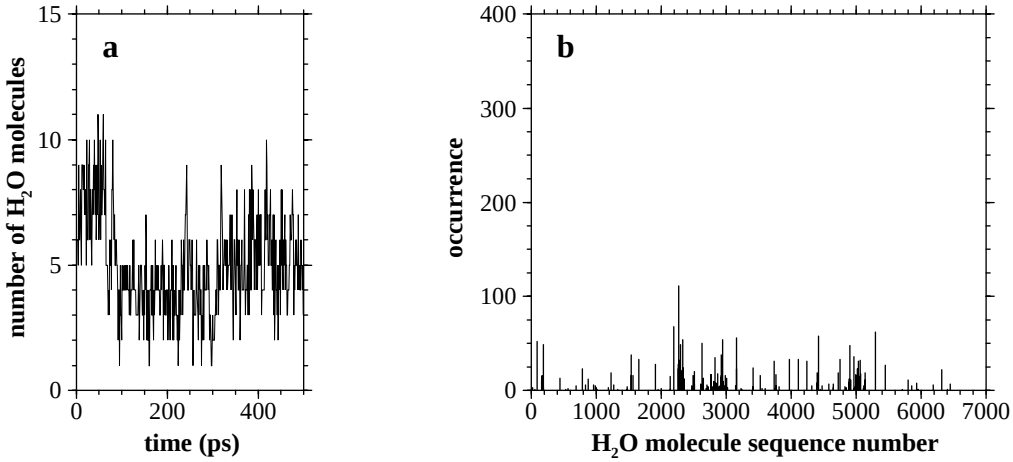

Figure 12. (a) Number of water molecules in the aryl-binding pocket as a function of simulation time. A water molecule was considered to be in the aryl-binding pocket if the distance between its oxygen and each of the Cβ atoms of Tyr-99, Phe-174 and Trp-215 was smaller than 0.9 nm. (b) Number of times each of the water molecules in the system has been found in the aryl-binding pocket in 500 system configurations taken at 1 ps intervals. Simulation with local-elevation interaction (see Methods).

sites are at hydrogen-bonding distance from 96Lys-O, 97Glu-O, 99Tyr-OηHη, and 175Ile-O. A less well-defined water site is at hydrogen-bonding distance from 98Thr-O. A water molecule is trapped most of the simulation time in the space defined between Ser-172, Phe-174, and Ile-175, although with a somewhat delocalised position. Conserved water sites in the trail to the specificity site are at hydrogen-bonding distance from 192Gln-Nϵ_2, 216Gly-NH, 216Gly-O, 217Glu-Oϵ, 218Gly-NH, and 189Asp-Oδ. In principle, these are sites which could be replaced by, or bridge, interactions with an inhibitor of new design. The agreement and degree of overlap between the data presented here and that obtained from the analysis of the crystallographic structures of two factor-Xa/inhibitor complexes and mutation data strengthens the position of MD-simulation techniques as an effective tool in the study of the active site of an enzyme prior to the application of specific drug-design techniques.

Acknowledgements

The authors wish to thank the second reviewer of the first submitted version of the manuscript for his or her valuable comments.

References

1. Mann, K.G., Nesheim, M.E., Church, W.R., Haley, P. and Krishnaswamy, S., Blood, 76 (1990) 1.
2. Kunitada, S. and Nagahara, T., Curr. Pharm. Design, 2 (1996) 531.
3. Kaiser, B. and Hauptmann, J., Cardiovasc. Drug Rev., 12 (1994) 225.
4. Sitko, G.R., Ramjit, D.R., Stabilito, I.I., Lehman, D., Lynch, J.J. and Vlasuk, G.P., Circulation, 85 (1992) 805.
5. Harker, L.A., Hanson, S.R. and Kelly, A.B., Thromb. Haemost., 74 (1995) 464.
6. Nierodzik, M.L., Klepfish, A. and Karpatkin, S., Thromb. Haemost., 74 (1995) 282.
7. Grand, R.J.A., Turnell, A.S. and Grabham, P.W., Biochem. J., 313 (1996) 353.
8. Lee, K.R., Betz, A.L., Keep, R.F., Chenevert, T.L., Kim, S. and Hoff, J.T., J. Neurosurg., 83 (1995) 1045.
9. Teo, M., Manser, E. and Lim, L., J. Biol. Chem., 270 (1995) 26690.
10. Brewer, G.J., Brain Res., 683 (1995) 258.
11. Padmanabhan, K., Padmanabhan, K.P., Tulinsky, A., Park, C.H., Bode, W., Huber, R., Blankenship, D.T., Cardin, A.D. and Kisiel, W., J. Mol. Biol., 232 (1993) 947.
12. Brandstetter, H., Kühne, A., Bode, W., Huber, R., von der Saal, W., Wirthensohn, K. and Engh, R.A., J. Biol. Chem., 271 (1996) 29988.
13. Kamata, K., Kawamoto, H., Honma, T., Iwama, T. and Kim, S.-H., Proc. Natl. Acad. Sci. USA, 95 (1998) 6630.
14. Stenflo, J., Crit. Rev. Euk. Gene Exp., 9 (1999) 59.
15. Birktoft, J.J. and Blow, D.M., J. Mol. Biol., 68 (1972) 187.
16. Tsukada, H. and Blow, D.M., J. Mol. Biol., 184 (1985) 703.
17. Skrzypczak-Jankun, E., Carperos, V.E., Ravichandran, K.G., Tulinsky, A., Westbrook, M. and Maraganore, J.M., J. Mol. Biol., 221 (1991) 1379.
18. Rydel, T.J., Tulinsky, A., Bode, W. and Huber, R., J. Mol. Biol., 221 (1991) 583.
19. Rezaie, A.R. and Esmon, C.T., J. Biol. Chem., 270 (1995) 16176.

20. Rezaie, A.R. and Esmon, C.T., Eur. J. Biochem., 242 (1996) 477.
21. Stubbs, M.T., Curr. Pharm. Design, 2 (1996) 543.
22. Shaw, K.J., Guilford, W.J., Dallas, J.L., Koovakkaat, S.K., McCarrick, M.A., Liang, A., Light, D.R. and Morrissey, M.M., J. Med. Chem., 41 (1998) 3551.
23. Bode, W., Brandstetter, H., Mather, T. and Stubbs, M.T., Thromb. Haemost., 78 (1997) 501.
24. Bode, W. and Schwager, P., J. Mol. Biol., 98 (1975) 693.
25. Internet address: http://wos.isiglobalnet.com/
26. Fraternali, F., Do, Q.-T., Doan, B.-T., Atkinson, R.A., Palmas, P., Sklenar, V., Safar, P., Wildgoose, P., Strop, P. and Saudek, V., Proteins Struct. Funct. Genet., 30 (1998) 264.
27. Ewing, W.R., Becker, M.R., Manetta, V.E., Davis, R.S., Pauls, H.W., Mason, H., Choi-Sledeski, Y.M., Green, D., Cha, D., Spada, A.P., Cheney, D.L., Mason, J.S., Maignan, S., Guilloteau, J.-P., Brown, K., Colussi, D., Bentley, R., Bostwick, J., Kasiewski, C.J., Morgan, S.R., Leadley, R.J., Dunwiddie, C.T., Perrone, M.H. and Chu, V., J. Med. Chem., 42 (1999) 3557.
28. Rao, M.S. and Olson, A.J., Proteins Struct. Funct. Genet., 34 (1999) 173.
29. Böhm, M., Stürzebecher, J. and Klebe, G., J. Med. Chem., 42 (1999) 458.
30. Vaz, R.J., McLean, L.R. and Pelton, J.T., J. Comput.-Aided Mol. Design, 12 (1998) 99.
31. McDowell, L.M., McCarrick, M.A., Studelska, D.R., Guilford, W.J., Arnaiz, D., Dallas, J.L., Light, D.R., Whitlow, M. and Schaefer, J., J. Med. Chem., 42 (1999) 3910.
32. Whitlow, M., Arnaiz, D.O., Buckman, B.O., Davey, D.D., Griedel, B., Guilford, W.J., Koovakkat, S.K., Liang, A., Mohan, R., Phillips, G.B., Seto, M., Shaw, K.J., Xu, W., Zhao, Z., Light, D.R. and Morrissey, M.M., Acta Crystallogr., D55 (1999) 1395.
33. Rezaie, A.R., J. Biol. Chem., 271 (1996) 23807.
34. Huber, T., Torda, A.E. and van Gunsteren, W.F., J. Comput.-Aided Mol. Design, 8 (1994) 695.
35. van Gunsteren, W.F., Billeter, S.R., Eising, A.A., Hünenberger, P.H., Krüger, P., Mark, A.E., Scott, W.R.P. and Tironi, I.G., Biomolecular Simulation: The GROMOS96 Manual and User Guide, Vdf Hochschulverlag AG an der ETH Zürich, Zürich, 1996.
36. Daura, X., Mark, A.E. and van Gunsteren, W.F., J. Comput. Chem., 19 (1998) 535.
37. Boschcov, P., Seidel, W., Muradian, J., Tominaga, M., Paiva, A.C.M. and Juliano, L., Bioorg. Chem., 12 (1983) 34.
38. Berendsen, H.J.C., Postma, J.P.M., van Gunsteren, W.F. and Hermans, J., In Pullman, B. (Ed.), Intermolecular Forces, D. Reidel Publ. Co., Dordrecht, The Netherlands, 1981, pp. 331–342.
39. Berendsen, H.J.C., Postma, J.P.M., van Gunsteren, W.F., DiNola, A. and Haak, J.R., J. Chem. Phys., 81 (1984) 3684.
40. Ryckaert, J.-P., Ciccotti, G. and Berendsen, H.J.C., J. Comput. Phys. 23 (1977) 327.
41. Scott, W.R.P., Hünenberger, P.H., Tironi, I.G., Mark, A.E., Billeter, S.R., Fennen, J., Torda, A.E., Huber, T., Krüger, P. and van Gunsteren, W.F., J. Phys. Chem. A, 103 (1999) 3596.
42. Laskowski, R.A., MacArthur, M.W., Moss, D.S. and Thornton, J.M., J. Appl. Crystallogr., 26 (1993) 283.
43. Smith, P.E. and van Gunsteren, W.F., J. Chem. Phys., 100 (1994) 3169.
44. Hünenberger, P.H., Mark, A.E. and van Gunsteren, W.F., J. Mol. Biol., 252 (1995) 492.
45. Kabsch, W. and Sander, C., Biopolymers, 22 (1983) 2577.
46. Renatus, M., Engh, R.A., Stubbs, M.T., Huber, R., Fischer, S., Kohnert, U. and Bode, W., EMBO J., 16 (1997) 4797.
47. Renatus, M., Stubbs, M.T., Huber, R., Bringmann, P., Donner, P., Schleuning, W.-D. and Bode, W., Biochemistry, 36 (1997) 13483.
48. Lamba, D., Bauer, M., Huber, R., Fischer, S., Rudolph, R., Kohnert, U. and Bode, W., J. Mol. Biol., 258 (1996) 117.
49. Renatus, M., Bode, W., Huber, R., Stürzebecher, J., Prasa, D., Fischer, S., Kohnert, U. and Stubbs, M.T., J. Biol. Chem., 272 (1997) 21713.